AIMS Mathematics, 11(11): 37735–37763.
DOI: 10.3934/math.20261459
Received: 19 May 2026
Revised: 02 September 2026
Accepted: 14 September 2026
Published: 13 November 2026

https://www.aimspress.com/journal/Math

Research article

Drift-implicit scheme for fractional stochastic volatility models with non-Lipschitz diffusion

Minoo Kamrani[1] **and Kristian Debrabant**[2,*]

[1] School of Mathematics, Statistics, and Computer Science, College of Science, University of Tehran, Tehran, Iran

[2] Department of Mathematics and Computer Science (IMADA), University of Southern Denmark, Campusvej 55, 5230 Odense M, Denmark

* **Correspondence:** Email: debrabant@imada.sdu.dk.

Abstract: In this study, we aim to approximate the solution of a general class of stochastic differential equations (SDEs) driven by fractional Brownian motion with a Hurst parameter $H > \frac{1}{2}$ and a square-root term in the diffusion coefficient. We employ the drift-implicit Euler-Maruyama (DIEM) method to approximate solutions of these SDEs and investigate its strong convergence properties. Despite the challenges posed by the non-Lipschitz diffusion coefficient, we demonstrate that, under reasonable monotonicity, regularity and moment assumptions on the drift function, the DIEM is mean-square convergent of order 1 for the Lamperti-transformed process, which is an optimal order. For the original square-root process $Y = X^2$, we obtain strong convergence of order 1 at the grid points. To demonstrate the practical relevance and computational efficiency of the method, we apply it to the fractional Cox-Ingersoll-Ross (CIR) model and discuss a fractional Heston-3/2 model whose reciprocal is a fractional CIR process. These applications underscore the potential of the proposed scheme in solving complex problems in computational statistics and finance, where fractional dynamics are used to model long-range dependencies and market memory.

Keywords: fractional Brownian motion; non-Lipschitz coefficients; drift-implicit scheme; CIR model; Heston-3/2 volatility; strong convergence; computational finance
Mathematics Subject Classification: 60G22, 60H35, 65C30, 91B70, 91-10

1. Introduction

Stochastic differential equations (SDEs) are fundamental in modeling dynamic systems subject to random fluctuations. Their wide-ranging applications in diverse fields, including economics, finance, mechanics, and more, have attracted significant attention from researchers [1–3].

As is well-known, many crucial equations in various applications possess coefficients that do not satisfy the global Lipschitz condition, making it essential to investigate a more general setting. Consequently, considerable research has been directed toward developing numerical schemes that remain valid within restricted domains for SDEs with non-Lipschitz continuous coefficients [4–6]. A classical and effective technique involves the application of a suitable Lamperti transform to convert the SDE into one with a constant diffusion coefficient, thus transferring all the non-smoothness to the drift term. This transformation is particularly useful for SDEs with non-globally Lipschitz coefficients and has, in particular, been successfully employed by Alfonsi [7] in the numerical treatment of the Cox-Ingersoll-Ross (CIR) process. Several financial models feature diffusion coefficients with square roots, which are non-globally Lipschitz, including the well-known CIR model [8].

SDEs driven by fractional Brownian motion (fBm) have attracted considerable attention from researchers [9, 10]. In financial modeling, fBm has been used to model temporal dependence in volatility. Gatheral et al. [11] showed that log-volatility behaves approximately like a fractional Brownian motion with a small Hurst parameter $H < \frac{1}{2}$, while Wang et al. [12] proposed a fractional Ornstein-Uhlenbeck model for realized volatility forecasting, also finding evidence of rough sample paths with $H < \frac{1}{2}$. These rough volatility models, however, lie outside the mathematical framework considered in this paper, which focuses on the regime $H > \frac{1}{2}$, i.e., persistent or long-memory dynamics. Long-memory stochastic-volatility models have been studied, e.g., in [13–15], including applications to option pricing and the estimation of volatility from financial data. In [16], a fractional Heston model with $H > \frac{1}{2}$ was developed and applied to derive option prices and implied volatilities. In [17], strict positivity of a fractional CIR-process has been proven for $H > \frac{1}{2}$, and in [18], a fractional Heston model was applied to the numerical approximation of option prices.

However, despite the increasing attention devoted to this area, the availability of numerical approximation methods for these equations remains limited, with only a few approaches to address the challenges posed by fBm.

Most researchers have investigated SDEs with fBms whose coefficients are globally Lipschitz [19–21]. The numerical approximation of fractional SDEs with non-Lipschitz coefficients presents unique challenges compared to the standard Brownian motion framework. Standard explicit Euler schemes are known to suffer from stability issues; they often fail to preserve the positivity of the solution, which is a strict requirement for volatility models like CIR, and can diverge in the strong sense when coefficients grow superlinearly. To overcome this, tamed and truncated Euler schemes have been proposed for fractional SDEs [22, 23]. While these methods restore strong convergence, they generally do not inherently guarantee pathwise positivity without modifications.

Implicit treatment of the drift is attractive for equations with singular or stiff transformed drifts, since it can improve stability and, for important models such as the fractional CIR equation, preserve positivity of the numerical approximation. Compared with explicit schemes, the additional per-step cost of a drift-implicit method stems from solving a generally nonlinear implicit equation, typically by an iterative nonlinear solver. When the implicit equation can be solved in closed form, as in the two CIR-type examples considered in Section 5, no iterative nonlinear solver is required.

Among the numerical methods for SDEs with non-Lipschitz or singular coefficients, several approaches are closely related to this work. For the fractional CIR model with $H \in (1/2, 1)$, Hong et al. [24] applied a backward-Euler-type scheme to the Lamperti-transformed equation and proved positivity and strong convergence of order one for the transformed process and, after

transforming back, for the original CIR process.

Related positivity-preserving numerical approaches for the CIR model include the adaptive splitting scheme proposed in [25]. For a class of additive SDEs characterized by a locally Lipschitz drift that is unbounded in the neighborhood of the origin, Zhang and Yuan [26] studied an implicit Euler approximation and obtained convergence of order H. Di Nunno et al. [27] investigated a drift-implicit Euler scheme for SDEs with unbounded drift driven by an arbitrary λ-Hölder continuous process and established convergence of order λ, which yields order H in the case of fractional Brownian motion.

An alternative approach for the fractional CIR model was proposed by Gao et al. [22], who introduced a positivity-preserving truncated Euler-Maruyama scheme and established strong convergence of order H. Related truncation-based methods for fractional Brownian motion-driven SDEs with nonlinear coefficients were studied by He et al. [23].

On the analytical side, Hu, Nualart, and Song [9] established existence and uniqueness results for singular stochastic differential equations driven by fractional Brownian motion. In particular, under suitable assumptions on the drift, their framework covers equations of the form

$$\begin{aligned} &\mathrm{d}Y(t) = f_1(Y(t))\mathrm{d}t + \sqrt{Y(t)}\mathrm{d}B^H(t), \qquad t \in [0,T], \\ &Y(0) = y_0 > 0, \end{aligned} \tag{1.1}$$

where $T > 0$ and $B^H(t)$ denotes a fBm with Hurst parameter $H \in (\frac{1}{2}, 1)$. Equation (1.1) is stated in the normalized form with unit diffusion scale. In Section 3, we consider the corresponding scaled model with a constant factor $\sigma > 0$ in the diffusion coefficient.

This paper provides an efficient numerical scheme for approximating solutions of the general SDE (1.1), focusing on SDEs with square-root diffusion, including the fractional CIR model, and showing how the fractional Heston-3/2 volatility model can be treated within the same framework via its reciprocal process. The main contribution of this paper is to extend the strong order-one analysis of drift-implicit discretizations beyond the specific fractional CIR drift treated in [24]. We consider the more general class of square-root diffusion models in (1.1), with a general drift function f_1 satisfying Assumptions 3.1–3.4 given in Section 3, and prove mean-square convergence of order one for the Lamperti-transformed process. We also establish strong order-one convergence in L^1 for the original process $Y = X^2$. For the fractional Heston-3/2 model, whose inverse-square transformation is singular at the origin, we derive a separate order-one result under additional inverse-moment conditions on the exact and numerical transformed solutions. The choice of fractional Brownian motion with Hurst parameter $H \in (1/2, 1)$ enables the model to represent persistence and long-range dependence, which can be relevant for financial quantities such as volatility and interest rates. The strong convergence result of order one provides accurate pathwise approximations of the fractional CIR and Heston-3/2-type processes. Such approximations can also be used to estimate functionals of the underlying financial process. In Section 5, we illustrate this by considering the integrated-short-rate functional

$$D(0,T) = \mathbb{E}\left(e^{-\int_0^T Y_s ds}\right)$$

and studying its numerical approximation for different time-step sizes.

However, we do not aim to develop a complete arbitrage-free pricing or forecasting framework. A systematic treatment of option pricing, volatility-surface calibration, or risk-measure evaluation would require additional modeling components and is beyond the scope of this work. The numerical

experiments are primarily designed to validate the theoretically predicted convergence behavior of the proposed drift-implicit Euler-Maruyama (DIEM) method and to illustrate its implications for a financially relevant functional. The analysis is restricted to one-dimensional fractional models with $H \in (1/2, 1)$ and square-root-type diffusion coefficients under the assumptions stated in the paper. More specifically, the convergence analysis relies essentially on the monotonicity of the Lamperti-transformed drift, together with the regularity and moment conditions introduced in Section 3. Although the DIEM scheme attains the optimal strong order one within this framework, extending the drift-implicit analysis to higher-order methods for fractional equations with singular or non-Lipschitz coefficients would require additional regularity and higher-order pathwise expansions and is beyond the scope of this work.

The article is organized as follows: In Section 2, we concisely review essential aspects related to fractional Brownian motion and Malliavin calculus for fBms. In Section 3, we present a detailed explanation of the problem under consideration, outlining the mathematical formulation and conditions for the existence of the solution. Section 4 is dedicated to the thorough convergence analysis of the DIEM scheme for SDEs driven by fBms with a square-root term. Furthermore, the strong convergence rate of the proposed method is obtained. Finally, in Section 5, we demonstrate the practical application of our approach, presenting outcomes and findings from numerical experiments on examples such as the CIR and Heston-3/2 volatility models, and showing the effectiveness and accuracy of our numerical scheme in financially motivated examples.

2. Preliminaries

Consider a filtered probability space $(\Omega, \mathcal{F}, (\mathcal{F}_t)_{t\geq 0}, \mathbb{P})$, and let $B^H = (B^H(t))_{t\geq 0}$ be a one-dimensional standard $(\mathcal{F}_t)$-adapted fractional Brownian motion with Hurst parameter $H \in (\frac{1}{2}, 1)$. A centered Gaussian stochastic process $\{B^H(t) : t \geq 0\}$ with Hurst parameter H is defined such that $\mathbb{E}(B^H(t)) = 0$, and its covariance function is expressed as

$$R_H(t, s) := \mathbb{E}(B^H(t)B^H(s)) = \frac{1}{2}\left(t^{2H} + s^{2H} - |t - s|^{2H}\right). \tag{2.1}$$

For $H = \frac{1}{2}$, $B^H(t)$ represents standard Brownian motion. The covariance function (2.1) implies that the increment of the process within an interval $[s, t]$ follows a normal distribution with zero mean and variance given by

$$\mathbb{E}\left(B^H(t) - B^H(s)\right)^2 = |t - s|^{2H}.$$

Malliavin analysis for fractional Brownian motion. In this section, we explore fundamental aspects of fractional Brownian motion [9]. The set $\mathcal{E}$ is defined as a collection of step functions on the interval $[0, T]$, and the associated Hilbert space $\mathcal{H}$ is constructed by closing $\mathcal{E}$ under the scalar product

$$< \mathbf{1}_{[0,t]}, \mathbf{1}_{[0,s]} >_{\mathcal{H}} := R_H(t, s).$$

To establish an isometry between $\mathcal{H}$ and its corresponding Gaussian space, we extend the mapping $\mathbf{1}_{[0,t]} \to B^H(t)$. This isometry, denoted as $u \to B^H(u)$ for $u \in \mathcal{H}$, satisfies, for any $u, v \in \mathcal{H}$,

$$< u, v >_{\mathcal{H}} = \int_0^T (K^* u)(s)(K^* v)(s)\mathrm{d}s,$$

where K^* is a linear operator from $\mathcal{E}$ to $L^2([0,T])$ defined as

$$(K^*u)(t_2) = \int_{t_2}^{T} u(t_1)\frac{\partial K_H}{\partial t_1}(t_1,t_2)\mathrm{d}t_1,\ u \in \mathcal{E}, t_2 \in [0,T],$$

and $K_H(t_1,t_2)$ takes the form

$$K_H(t_1,t_2) := c_H t_2^{\frac{1}{2}-H}\int_{t_2}^{t_1}(t-t_2)^{H-\frac{3}{2}}t^{H-\frac{1}{2}}\mathrm{d}t\mathbf{1}_{\{t_2<t_1\}},$$

with

$$c_H := \sqrt{\frac{\alpha_H}{\beta(2-2H,H-\frac{1}{2})}},$$

where $\alpha_H = H(2H-1)$ and $\beta(\cdot,\cdot)$ is the Beta function.

Definition 2.1. Consider a function $f \in C_b^\infty(\mathbb{R}^n)$. Let F denote a smooth random variable defined as $F = f(B^H(t_1),...,B^H(t_n))$. The derivative process of F is denoted by the $\mathcal{H}$-valued random variable D_sF, where

$$D_sF := \sum_{i=1}^{n}\frac{\partial f}{\partial x_i}(B^H(t_1),\ldots,B^H(t_n))\mathbf{1}_{[0,t_i]}(s), \quad s \in [0,T].$$

Notably, for the fractional Brownian motion $B^H(t)$, we express $D_sB^H(t) = \mathbf{1}_{[0,t]}(s)$.

Furthermore, let $\mathbb{D}^{1,2}$ be the completion of the class of smooth random variables with respect to the norm

$$|G|_{\mathbb{D}^{1,2}} := \left(\mathbb{E}[|G|^2] + \mathbb{E}[|DG|_{\mathcal{H}}^2]\right)^{\frac{1}{2}}.$$

Let δ denote the adjoint of the operator D. The Skorohod integral of g with respect to fractional Brownian motion is introduced as

$$\int_0^T g(t)\delta B^H(t) := \delta(g),$$

and this yields

$$\mathbb{E}\left[\int_0^T g(t)\delta B^H(t)\right] = 0.$$

Moreover, for $t \in [0,T]$, the expression $\int_0^t g(u)\delta B^H(u) := \delta(g\mathbf{1}_{[0,t]})$ is defined. Notably, the definition of $\mathbb{D}^{1,2}$ can be extended to $\mathbb{D}^{1,2}(\mathcal{H})$ for $\mathcal{H}$-valued random variables, and this space is contained in $Domain(\delta)$.

Furthermore, we have

$$\int_0^t g(s)\mathrm{d}B^H(s) = \int_0^t g(s)\delta B^H(s) + \int_0^t\int_0^T D_\varsigma g(s)\varrho(\varsigma,s)\,d\varsigma\,ds, \tag{2.2}$$

where the integral on the left side is the Riemann-Stieltjes integral and

$$\varrho(\varsigma,s) = \alpha_H|\varsigma - s|^{2H-2}. \tag{2.3}$$

Lemma 2.1. *[9] Let $pH > 1$ and denote $\mathbb{L}_{\mathcal{H}}^{1,p} := \left\{g \in \mathbb{D}^{1,2}(\mathcal{H}) : \|g\|_{p,1} < \infty\right\}$, where*

$$\|g\|_{p,1}^p := \int_0^T \mathbb{E}[|g(u)|^p]\mathrm{d}u + \mathbb{E}\left[\int_0^T \left(\int_0^T |D_\varsigma g(u)|^{\frac{1}{H}}\mathrm{d}\varsigma\right)^{pH} \mathrm{d}u\right].$$

If a process $g \in \mathbb{L}_{\mathcal{H}}^{1,p}$, then

$$\mathbb{E}\left[\sup_{0\le t\le T}\left|\int_0^t g(u)\delta B^H(u)\right|^p\right] \le C(T,H,p)\|g\|_{p,1}^p.$$

3. Problem formulation and drift-implicit discretization

Model, Lamperti transformation, and existence. Consider the following SDE:

$$\begin{aligned} &\mathrm{d}Y(t) = f_1(Y(t))\mathrm{d}t + \sigma\sqrt{Y(t)}\mathrm{d}B^H(t), \quad t \in [0,T],\\ &Y(0) = y_0, \end{aligned} \tag{3.1}$$

where $T > 0$, $y_0 > 0$, and $B^H(t)$ is a fractional Brownian motion with Hurst parameter $H \in (\frac{1}{2}, 1)$.

Assumption 3.1. *Assume that $f_1 \in C^1((0,\infty))$ and*

$$2yf_1'(y) \le f_1(y), \ \ \forall y > 0.$$

Remark 3.1. *The rationale for Assumption 3.1 is structural: It ensures that the drift $f(x)$ of the Lamperti-transformed process $X(t) = \sqrt{Y(t)}$ satisfies the one-sided monotonicity condition $f'(x) \le 0$ for all $x > 0$. Thus, the drift of the Lamperti-transformed equation is non-increasing, a property that is essential for the stability estimate in the convergence analysis. For example, in the CIR model where $f_1(y) = K(\theta - y)$ with $K, \theta > 0$, Assumption 3.1 reduces to $-2Ky \le K(\theta - y)$, which is satisfied for all $y > 0$.*

Applying the Young chain rule to the positive stochastic process $Y = (Y(t), t \ge 0)$, with $X(t) = \sqrt{Y(t)}$, we find that $Y(t)$ satisfies (3.1) if and only if $X(t)$ satisfies the following equation:

$$\begin{aligned} &\mathrm{d}X(t) = f(X(t))\mathrm{d}t + \frac{\sigma}{2}\mathrm{d}B^H(t), \quad t \in [0,T],\\ &X(0) = x_0 = \sqrt{y_0}, \end{aligned} \tag{3.2}$$

where $f(x) = \frac{f_1(x^2)}{2x}$.

Although fractional Brownian motion B^H is neither a Markov process nor a semimartingale, applying the Lamperti transformation reduces the non-Lipschitz diffusion to an additive fractional noise. This simplification enables stochastic integrals to be well-defined in a pathwise sense, while our strong convergence analysis uses Malliavin calculus to handle non-Markovian error propagation.

The following theorem introduces conditions that ensure the existence of solutions for (3.1) and (3.2).

Theorem 3.1. *[9] Suppose that Assumption 3.1 holds and that $f_1(y) \geq 0$ for all $y > 0$. Assume also that there exist constants $c > 0$, $y_* > 0$, and*

$$q < 1 - \frac{1}{2H}$$

such that

$$f_1(y) \geq cy^q, \qquad 0 < y < y_*. \tag{3.3}$$

Then Eq (3.2) *has a unique pathwise solution $X(t)$ such that $X(t) > 0$ almost surely on $[0, \infty)$. Consequently, $Y(t) = X(t)^2$ is the unique strictly positive pathwise solution of* (3.1)*.*

Regularity assumptions for the convergence analysis. Theorem 3.1 provides sufficient conditions for existence and strict positivity of the exact solution. For the strong convergence analysis of the numerical method, we also require the following regularity and moment assumptions on the Lamperti-transformed solution.

Assumption 3.2. *Assume that $f \in C^2((0, \infty))$ and that Eq* (3.2) *admits a unique pathwise solution $X(t)$ such that $X(t) > 0$ almost surely on $[0, T]$ and*

$$\sup_{t\in[0,T]} \mathbb{E}|f'(X(t))|^2 + \sup_{t\in[0,T]} \mathbb{E}|f'(X(t))f(X(t))|^2 + \sup_{t\in[0,T]} \mathbb{E}|f''(X(t))|^2 < \infty.$$

Remark 3.2. *Assumption 3.2 requires the boundedness of specific moments involving the transformed drift and its derivatives evaluated at the exact solution. This is a technical necessity to bound the truncation errors and Malliavin derivatives in the proof of the strong convergence rate in Theorem 4.1. Although assuming bounds on the exact solution may appear abstract, it is not overly restrictive for practical financial applications. As demonstrated in Examples 5.1 and 5.2, the required moment bounds are naturally satisfied for the CIR-type equations provided that a generalized Feller-type condition holds, which restricts the parameters such that the process does not accumulate near zero. The fractional Heston-3/2 model is treated separately in Example 5.3 and Corollary 5.1, where additional inverse-moment bounds are imposed to control the singular inverse-square transformation.*

Assumption 3.3. *For every $t \in [0, T]$, the solution $X(t)$ belongs to $\mathbb{D}^{1,2}$. Moreover, for $0 \leq \varsigma \leq t \leq T$, its Malliavin derivative satisfies*

$$D_\varsigma X(t) = \frac{\sigma}{2} + \int_\varsigma^t f'(X(u))D_\varsigma X(u)\, du, \tag{3.4}$$

whereas $D_\varsigma X(t) = 0$ for $\varsigma > t$.

Remark 3.3. *Assumption 3.3 is a standard regularity property for fractional SDEs with additive noise. For equations with regular coefficients, Malliavin differentiability and the corresponding variational equation follow from standard results; see, e.g., [10]. For singular equations with additive fractional Brownian noise, corresponding results are established in [9]. In particular, this covers the drift $f(x) = K/x$ considered in Example 5.1. For the fractional CIR equation considered in Example 5.2, the Malliavin derivative is given explicitly in [24]. Hence, Assumption 3.3 is satisfied for the principal examples considered below;* (5.14) *reduces to the same CIR-type transformed equation.*

The DIEM scheme and well-posedness. The primary challenge in model (3.2) is the severe stiffness introduced by the Lamperti-transformed drift, which can cause standard explicit schemes to oscillate and fail to preserve the strict positivity of the underlying volatility process. Therefore, we isolate this difficulty by treating the drift implicitly. Because the fractional noise becomes additive after the transformation, the non-Markovian dependence structure of the fBm does not alter the algebraic form of the implicit solve at an individual time step.

Applying the DIEM method to Eq (3.2), we obtain the following numerical scheme:

$$X_{k+1} = X_k + f(X_{k+1})\Delta + \frac{\sigma}{2}\Delta B_k^H, \quad k = 0, 1, \ldots, N-1, \tag{3.5}$$

where $X_0 = x_0$, $N \in \mathbb{N}$ is the number of time steps, $\Delta = \frac{T}{N} > 0$ represents the time discretization step-size, $t_k = k\Delta$ for $k = 0, 1, \ldots, N$, and

$$\Delta B_k^H = B^H((k+1)\Delta) - B^H(k\Delta). \tag{3.6}$$

The following assumption guarantees that the implicit equation in (3.5) is well posed on $(0, \infty)$.

Assumption 3.4. *There exists $\Delta_0 > 0$ such that, for every $\Delta \in (0, \Delta_0]$, the function*

$$\Phi_\Delta(x) := x - \Delta f(x), \qquad x > 0,$$

satisfies

$$\lim_{x \downarrow 0} \Phi_\Delta(x) = -\infty, \qquad \lim_{x \to \infty} \Phi_\Delta(x) = +\infty.$$

Remark 3.4. *By Assumption 3.1, $\Phi'_\Delta(x) = 1 - \Delta f'(x) \geq 1$ for $x > 0$. Together with Assumption 3.4, which, by continuity, ensures that Φ_Δ maps $(0, \infty)$ onto $\mathbb{R}$, this implies that the implicit equation in* (3.5) *admits a unique positive solution at every time step. Both CIR-type examples considered in Section 5 satisfy this condition; in fact, in these cases, the unique positive solution is available in closed form. Moreover, if the assumptions of Theorem 3.1 hold, Assumption 3.4 is fulfilled.*

Thus, Assumptions 3.1 and 3.4 ensure that the DIEM recursion is pathwise well defined and strictly positive at every time step. Together with Assumptions 3.2 and 3.3, these conditions form the framework for the convergence analysis in the next section.

4. Convergence of the proposed numerical scheme

Our main aim in this section is to investigate the convergence and the strong convergence rate of the numerical scheme (3.5). Throughout this section, C denotes a generic constant that is independent of Δ, but may depend on T, H, σ and may change from line to line.

Theorem 4.1. *Let $T > 0$, and suppose Assumptions 3.1–3.4 hold. Let $X(k\Delta)$ denote the solution of SDE* (3.2)*, and X_k be the numerical solution obtained using the DIEM scheme* (3.5) *at the grid point $t_k = k\Delta$. Then, there exists a constant $C > 0$ such that*

$$\mathbb{E}\left[\max_{k=0,\ldots,N} |X(k\Delta) - X_k|^2\right] \leq C\Delta^2.$$

Proof. The proof of the strong convergence result proceeds in four main steps. First, on each interval $[t_k, t_{k+1}]$, we use the integrated chain rule to decompose the local defect into a Lebesgue-integral contribution C^1_{k+1}, involving only ordinary time integrals, and a fractional-noise term C^2_{k+1}, involving an integral with respect to fBm. Second, Assumption 3.1 implies the monotonicity $f'(x) \leq 0$, which yields $\gamma_{k+1} \leq 0$ in the error recursion $e_{k+1} = e_k + e_{k+1}\gamma_{k+1}\Delta + C^1_{k+1} + C^2_{k+1}$. A discrete integrating factor is then used to obtain a stable representation of the accumulated global error. Third, the Young integral appearing in C^2_{k+1} is rewritten, using (2.2), as the sum of a Skorohod integral and a Malliavin correction term. Discrete summation by parts is subsequently used to control the accumulation of the Skorohod-integral increments. This leads to the decomposition of the global error into the three terms *I*, *II*, and *III* below. Finally, these terms are estimated separately: *I* is controlled by the moment bound on $f'(X)f(X)$, *II* by Lemma 2.1 together with a Malliavin-derivative estimate, and *III* by the moment bound on $f''(X)$. Together with the monotonicity condition in Assumption 3.1 and the Malliavin regularity in Assumption 3.3, Assumption 3.2 provides the moment bounds needed to complete these estimates.

Step 1. Local defect decomposition and error recursion

From Eq (3.2), we have

$$X(t_{k+1}) = X(t_k) + \int_{t_k}^{t_{k+1}} f(X(s))\mathrm{d}s + \frac{\sigma}{2}\Delta B^H_k, \;\; k = 0, 1, \ldots, N-1. \tag{4.1}$$

Since f is twice continuously differentiable, using the integrated chain rule, we deduce

$$f(X(s)) = f(X(t_{k+1})) - \int_s^{t_{k+1}} f(X(r))f'(X(r))\mathrm{d}r - \frac{\sigma}{2}\int_s^{t_{k+1}} f'(X(r))\mathrm{d}B^H_r. \tag{4.2}$$

By substituting (4.2) into (4.1), we obtain

$$X(t_{k+1}) = X(t_k) + f(X(t_{k+1}))\Delta + C^1_{k+1} + C^2_{k+1} + \frac{\sigma}{2}\Delta B^H_k, \tag{4.3}$$

where

$$C^1_{k+1} = -\int_{t_k}^{t_{k+1}}\int_s^{t_{k+1}} f(X(r))f'(X(r))\mathrm{d}r\mathrm{d}s,$$

and

$$C^2_{k+1} = -\frac{\sigma}{2}\int_{t_k}^{t_{k+1}}\int_s^{t_{k+1}} f'(X(r))\mathrm{d}B^H(r)\mathrm{d}s.$$

By subtracting (3.5) from (4.3), we obtain

$$X(t_{k+1}) - X_{k+1} = X(t_k) - X_k + (f(X(t_{k+1})) - f(X_{k+1}))\,\Delta + C^1_{k+1} + C^2_{k+1}, \tag{4.4}$$

which leads to

$$e_{k+1} = e_k + e_{k+1}\gamma_{k+1}\Delta + C^1_{k+1} + C^2_{k+1},$$

where $\gamma_{k+1} := \frac{f(X(t_{k+1}))-f(X_{k+1})}{X(t_{k+1})-X_{k+1}}$ if $X(t_{k+1}) \neq X_{k+1}$ and $\gamma_{k+1} := 0$ if $X(t_{k+1}) = X_{k+1}$.

Step 2. Stability and accumulation of the local errors

From Assumption 3.1 and the mean value theorem, we deduce $\gamma_{k+1} \leq 0$. Therefore,

$$(1 - \gamma_{k+1}\Delta)e_{k+1} = e_k + C^1_{k+1} + C^2_{k+1}. \tag{4.5}$$

Define $\zeta_0 := 1$ and $\zeta_k := \prod_{j=1}^{k}(1-\gamma_j\Delta)$. Multiplying both sides by ζ_k, we obtain

$$(1-\gamma_{k+1}\Delta)\prod_{j=1}^{k}(1-\gamma_j\Delta)e_{k+1} = \prod_{j=1}^{k}(1-\gamma_j\Delta)e_k + \prod_{j=1}^{k}(1-\gamma_j\Delta)\left(C_{k+1}^1 + C_{k+1}^2\right),$$

which leads to

$$\tilde{e}_{k+1} = \tilde{e}_k + \zeta_k(C_{k+1}^1 + C_{k+1}^2), \tag{4.6}$$

where $\tilde{e}_k := \zeta_k e_k$, implying that $\tilde{e}_k = \sum_{j=0}^{k-1}\zeta_j(C_{j+1}^1 + C_{j+1}^2)$ and thus

$$e_k = \frac{1}{\zeta_k}\sum_{j=0}^{k-1}\zeta_j(C_{j+1}^1 + C_{j+1}^2). \tag{4.7}$$

Step 3. Young-Skorohod decomposition of the fractional-noise error
Note that

$$C_{k+1}^1 = -\int_{t_k}^{t_{k+1}}(r-t_k)f(X(r))f'(X(r))\mathrm{d}r, \tag{4.8}$$

and from (2.2), we get

$$\begin{aligned} C_{k+1}^2 &= -\frac{\sigma}{2}\int_{t_k}^{t_{k+1}}(r-t_k)f'(X(r))\mathrm{d}B^H(r) \\ &= -\frac{\sigma}{2}\int_{t_k}^{t_{k+1}}(r-t_k)f'(X(r))\delta B^H(r) - \frac{\sigma}{2}\int_{t_k}^{t_{k+1}}\left(\int_0^T(r-t_k)D_\varsigma[f'(X(r))]\varrho(\varsigma,r)\,d\varsigma\right)dr. \end{aligned} \tag{4.9}$$

For $r \in [t_k, t_{k+1})$, denote $\lfloor r/\Delta \rfloor = k$. Define

$$\tilde{R}(t) := -\frac{\sigma}{2}\int_0^t (r - t_{\lfloor r/\Delta\rfloor})f'(X(r))\,\delta B^H(r). \tag{4.10}$$

Then, we obtain from (4.7)–(4.10)

$$\begin{aligned} e_k = &-\int_0^{t_k}\frac{\zeta_{\lfloor r/\Delta\rfloor}}{\zeta_k}(r-t_{\lfloor r/\Delta\rfloor})f'(X(r))f(X(r))\,dr + \sum_{j=0}^{k-1}\frac{\zeta_j}{\zeta_k}(\tilde{R}(t_{j+1}) - \tilde{R}(t_j)) \\ &-\int_0^{t_k}\int_0^T\frac{1}{2}\sigma\frac{\zeta_{\lfloor r/\Delta\rfloor}}{\zeta_k}(r-t_{\lfloor r/\Delta\rfloor})D_\varsigma[f'(X(r))]\varrho(\varsigma,r)\,d\varsigma\,dr. \end{aligned} \tag{4.11}$$

Applying discrete summation by parts to the Skorohod-integral increments, we obtain

$$\left|\sum_{j=0}^{k-1}\zeta_j(\tilde{R}(t_{j+1}) - \tilde{R}(t_j))\right| = \left|\zeta_{k-1}\tilde{R}(t_k) + \sum_{j=1}^{k-1}(\zeta_{j-1} - \zeta_j)\tilde{R}(t_j)\right| \le 2\zeta_{k-1}\sup_{1\le j\le k}|\tilde{R}(t_j)|.$$

Using $\frac{\zeta_j}{\zeta_k} \le 1$, $j = 1, \cdots, k$, we deduce

$$\mathbb{E}\left[\max_{0\le k\le N}|e_k|^2\right] \le C\left(\mathbb{E}\left[\left(\int_0^T|(r-t_{\lfloor r/\Delta\rfloor})f'(X(r))f(X(r))|\,dr\right)^2\right] + \mathbb{E}\left[\max_{1\le j\le N}|\tilde{R}(t_j)|^2\right]\right.$$

$$+\mathbb{E}\left[\left(\int_0^T\int_0^T\left|\frac{1}{2}\sigma(r-t_{\lfloor r/\Delta\rfloor})D_\varsigma[f'(X(r))]\varrho(\varsigma,r)\right|d\varsigma\,dr\right)^2\right]\Bigg)$$
$$=: C(I+II+III). \tag{4.12}$$

Step 4. Estimates of the three error contributions

We first record the Malliavin derivative estimate that will be used for II and III. Malliavin differentiability of solutions of fractional SDEs and the corresponding variational equation are discussed, for example, in [10]; see also [9] for singular equations with additive fractional Brownian noise.

For $0 \le \varsigma \le r$, applying the Malliavin derivative D_ς to the integral form of (3.2) gives

$$D_\varsigma X(r) = \frac{\sigma}{2} + \int_\varsigma^r f'(X(u))D_\varsigma X(u)\,du,$$

whereas $D_\varsigma X(r) = 0$ for $\varsigma > r$. Solving this linear variational equation yields

$$D_\varsigma X(r) = \frac{\sigma}{2}\exp\left(\int_\varsigma^r f'(X(u))\,du\right)\mathbf{1}_{[0,r]}(\varsigma). \tag{4.13}$$

By the chain rule of Malliavin calculus,

$$D_\varsigma[f'(X(r))] = f''(X(r))D_\varsigma X(r). \tag{4.14}$$

Since Assumption 3.1 implies that $f'(x) \le 0$ for all $x > 0$, and $X(\iota) > 0$ almost surely by Assumption 3.2, we have $\exp\left(\int_\varsigma^r f'(X(\iota))\,d\iota\right) \le 1$. Consequently, (4.13) and (4.14) imply

$$|D_\varsigma[f'(X(r))]| \le |f''(X(r))\frac{\sigma}{2}|\mathbf{1}_{[0,r]}(\varsigma). \tag{4.15}$$

For the first term I, using Minkowski's integral inequality, the estimate $|r - t_{\lfloor r/\Delta\rfloor}| \le \Delta$ and the moment bound on $f'(X(r))f(X(r))$ in Assumption 3.2, we get

$$\begin{aligned} I &= \left\|\int_0^T |(r-t_{\lfloor r/\Delta\rfloor})f'(X(r))f(X(r))|\,dr\right\|_{L^2(\Omega)}^2 \\ &\le \left(\int_0^T \|(r-t_{\lfloor r/\Delta\rfloor})f'(X(r))f(X(r))\|_{L^2(\Omega)}\,dr\right)^2 \\ &\le \Delta^2 \sup_{0\le r\le T}\|f'(X(r))f(X(r))\|_{L^2(\Omega)}^2 T^2 \le C\Delta^2. \end{aligned} \tag{4.16}$$

For the second term II, Lemma 2.1 with $p = 2$ yields

$$\begin{aligned} II &= \mathbb{E}\left[\max_{1\le j\le N}|\tilde{R}(t_j)|^2\right] \\ &\le C\int_0^T \mathbb{E}\left|\frac{1}{2}\sigma(r-t_{\lfloor r/\Delta\rfloor})f'(X(r))\right|^2 dr + C\mathbb{E}\left[\int_0^T\left(\int_0^T\left|\frac{1}{2}\sigma(r-t_{\lfloor r/\Delta\rfloor})D_\varsigma[f'(X(r))]\right|^{\frac{1}{H}}d\varsigma\right)^{2H}dr\right] \end{aligned}$$

$$\leq C\Delta^2 \int_0^T \mathbb{E}|f'(X(r))|^2 dr + C\Delta^2 \mathbb{E}\left[\int_0^T \left(\int_0^T \left|D_\varsigma[f'(X(r))]\right|^{\frac{1}{H}} d\varsigma\right)^{2H} dr\right].$$

Moreover, by (4.15),

$$\left(\int_0^T |D_\varsigma[f'(X(r))]|^{1/H} d\varsigma\right)^{2H} \leq \left(\frac{\sigma}{2}\right)^2 r^{2H}|f''(X(r))|^2,$$

implying that

$$II \leq C\Delta^2 \int_0^T \mathbb{E}|f'(X(r))|^2 dr + C\Delta^2 \int_0^T r^{2H}\mathbb{E}|f''(X(r))|^2 \, dr \leq C\Delta^2,$$

where we have used the uniform $L^2(\Omega)$-bounds on $f'(X(r))$ and $f''(X(r))$ in Assumption 3.2.

For the third term III, (4.15) and

$$\int_0^T \mathbf{1}_{[0,r]}(\varsigma)\varrho(\varsigma, r)\, d\varsigma = Hr^{2H-1} \leq HT^{2H-1}$$

give together with the uniform $L^2(\Omega)$-bound on $f''(X(r))$ from Assumption 3.2

$$\begin{aligned} III &\leq C\mathbb{E}\left[\left(\int_0^T (r - t_{\lfloor r/\Delta \rfloor})|f''(X(r))| \int_0^T \mathbf{1}_{[0,r]}(\varsigma)\varrho(\varsigma, r)d\varsigma\, dr\right)^2\right] \\ &\leq C\Delta^2\left(\int_0^T \|f''(X(r))\|_{L^2(\Omega)}\, dr\right)^2 \leq C\Delta^2. \end{aligned} \tag{4.17}$$

Combining the estimates for I, II, and III, we obtain

$$\mathbb{E}\left[\max_{0\leq k\leq N}|e_k|^2\right] \leq C\Delta^2, \tag{4.18}$$

which completes the proof.

Corollary 4.1. *Under the assumptions of Theorem 4.1, let $Y(t) = X^2(t)$ and let X_k be the numerical approximation obtained from* (3.5)*. Suppose also that $\mathbb{E}\left[\sup_{0\leq t\leq T}|X(t)|^2\right] < \infty$. Then, for any $T > 0$, there exists a constant C_T such that*

$$\mathbb{E}\left[\max_{0\leq k\leq N}|Y(t_k) - X_k^2|\right] \leq C_T\Delta. \tag{4.19}$$

Proof. By the algebraic identity $|a^2 - b^2| = |a - b||a + b|$ and the Cauchy-Schwarz inequality, we have

$$\begin{aligned} \mathbb{E}\left[\max_{0\leq k\leq N}|X^2(t_k) - X_k^2|\right] &\leq \mathbb{E}\left[\max_{0\leq k\leq N}|X(t_k) - X_k| \cdot \max_{0\leq k\leq N}|X(t_k) + X_k|\right] \\ &\leq \left(\mathbb{E}\left[\max_{0\leq k\leq N}|X(t_k) - X_k|^2\right]\right)^{1/2}\left(\mathbb{E}\left[\max_{0\leq k\leq N}|X(t_k) + X_k|^2\right]\right)^{1/2}. \end{aligned}$$

From Theorem 4.1, the first term is $O(\Delta)$. For the second term, we use the triangle inequality:

$$\left(\mathbb{E}\left[\max_{0\leq k\leq N}|X(t_k) + X_k|^2\right]\right)^{1/2} \leq \left(\mathbb{E}\left[\max_{0\leq k\leq N}|2X(t_k) + (X_k - X(t_k))|^2\right]\right)^{1/2}$$

$$\leq C\left(\mathbb{E}\left[\sup_{0\leq t\leq T}|X(t)|^2\right]\right)^{1/2} + C\left(\mathbb{E}\left[\max_{0\leq k\leq N}|X_k - X(t_k)|^2\right]\right)^{1/2}.$$

The first part is finite by the moment assumption on the exact solution X in Corollary 4.1, and the second part is $O(\Delta)$ by Theorem 4.1. Thus, the second term in the Cauchy-Schwarz inequality is bounded by a constant independent of Δ. Consequently, the strong convergence rate of order 1 is established for the process $Y(t)$.

5. Numerical results

In this section, we demonstrate the effectiveness of the theoretical results by applying the proposed numerical scheme (3.5) to some problems in mathematical finance.

Numerical error measures and confidence intervals. In the numerical experiments in this section, the exact solutions X of (3.2) and Y of (3.1) are unavailable. Therefore, we approximate them by reference solutions based on a fine-grid DIEM approximation with (unless stated otherwise) $N_* = 2^{15}$ time steps and time step size $\Delta_* = \frac{T}{N_*}$. For the coarser grids, we use $N_\ell = 2^\ell$, $\Delta_\ell = \frac{T}{N_\ell}$, $\ell = 6, \ldots, 10$.

By applying the covariance formula (2.1) to the fractional Brownian motion increments defined in (3.6), we obtain

$$\mathrm{Cov}(\Delta B_j^H, \Delta B_{j+k}^H) = \frac{\Delta_*^{2H}}{2}\left(|k+1|^{2H} - 2|k|^{2H} + |k-1|^{2H}\right).$$

To generate increments with this covariance structure, we use the Davies-Harte circulant-embedding method [28].

For each Monte Carlo path, the coarse-grid increments are obtained by summing the corresponding fine-grid increments, ensuring an exact coupling of the fine and coarse discretizations.

Unless stated otherwise, we use $M = 1000$ Monte Carlo sample paths to approximate expectations. The complete simulation procedure is summarized in Algorithm 1.

Algorithm 1 DIEM convergence experiments

Set Y_0 and T. Set $N_* = 2^{15}$, and $M = 1000$.
for $m = 1, \ldots, M$ **do**
    Generate the increments of a standard fractional Brownian motion on the reference grid using the Davies-Harte circulant-embedding method.
    Compute the reference DIEM solution.
    for $j = 6, \ldots, 10$ **do**
        Set $N = 2^j$ and $\Delta = \frac{T}{N}$.
        Construct coarse fBm increments by aggregating the corresponding reference-grid increments.
        Compute the coarse-grid DIEM solution.
        Record the errors against the reference solution at the corresponding coarse-grid points.
    end for
end for

We denote by $X_{\ell,k}^{(m)}$ the DIEM approximation for the mth Monte Carlo path on the grid with step size Δ_ℓ at time point $t_{\ell,k} = k\Delta_\ell$, $k = 0, \ldots, N_\ell$, and by $X^{*,m}(t_{\ell,k})$ the corresponding fine-grid reference approximation. For the original process Y, we define

$$Y_{\ell,k}^{(m)} = \left(X_{\ell,k}^{(m)}\right)^2, \qquad Y^{*,m}(t_{\ell,k}) = \left(X^{*,m}(t_{\ell,k})\right)^2.$$

For each path, we define the pathwise errors as

$$Q_\ell^{X,m} = \max_{0\le k\le N_\ell} \left|X_{\ell,k}^{(m)} - X^{*,m}(t_{\ell,k})\right|, \qquad Q_\ell^{Y,m} = \max_{0\le k\le N_\ell} \left|Y_{\ell,k}^{(m)} - Y^{*,m}(t_{\ell,k})\right|.$$

The corresponding Monte Carlo estimator for the root mean square error (RMSE) of the approximation to X is then given by

$$\widehat{\mathrm{Err}}_{X,2}(\Delta_\ell) = \left(\frac{1}{M}\sum_{m=1}^{M}\left(Q_\ell^{X,m}\right)^2\right)^{1/2},$$

while the Monte Carlo estimator for the strong error of the approximation of the original process Y is given by

$$\widehat{\mathrm{Err}}_{Y,1}(\Delta_\ell) = \frac{1}{M}\sum_{m=1}^{M} Q_\ell^{Y,m}.$$

For $\ell = 7, \ldots, 10$, we calculate the observed convergence orders as

$$\widehat{p}_{X,2}(\Delta_\ell) = \log_2\left(\frac{\widehat{\mathrm{Err}}_{X,2}(\Delta_{\ell-1})}{\widehat{\mathrm{Err}}_{X,2}(\Delta_\ell)}\right), \qquad \widehat{p}_{Y,1}(\Delta_\ell) = \log_2\left(\frac{\widehat{\mathrm{Err}}_{Y,1}(\Delta_{\ell-1})}{\widehat{\mathrm{Err}}_{Y,1}(\Delta_\ell)}\right).$$

To quantify the Monte Carlo sampling uncertainty, we use a batch average method (see [29]). We distribute the $M = 1000$ independent paths into $B = 20$ disjoint batches with $n = 50$ paths each, such that $M = Bn$. Denoting by I_b the index set of the b-th batch, we calculate the batch averages

$$\overline{Q_{\ell,b}^Y} = \frac{1}{n}\sum_{m\in I_b} Q_\ell^{Y,m}, \qquad b = 1, \ldots, B.$$

The mean of the batch means satisfies

$$\overline{Q_\ell^Y} = \frac{1}{B}\sum_{b=1}^{B}\overline{Q_{\ell,b}^Y} = \frac{1}{M}\sum_{m=1}^{M} Q_\ell^{Y,m}.$$

The sample variance of the batch averages is then given by

$$S_{\ell,B,Y}^2 = \frac{1}{B-1}\sum_{b=1}^{B}\left(\overline{Q_{\ell,b}^Y} - \overline{Q_\ell^Y}\right)^2.$$

The standard error of the overall mean value $\overline{Q_\ell^Y}$ can therefore be estimated by $\frac{S_{\ell,B,Y}}{\sqrt{B}}$. Assuming that the batch means are approximately normally distributed, we obtain the approximate 95% confidence interval

$$\left[\overline{Q_\ell^Y} - t_{B-1,0.975}\frac{S_{\ell,B,Y}}{\sqrt{B}},\ \overline{Q_\ell^Y} + t_{B-1,0.975}\frac{S_{\ell,B,Y}}{\sqrt{B}}\right]$$

for the expected pathwise error $\mathbb{E}[Q_\ell^{Y,1}]$ relative to the fine-grid reference solution, where $t_{B-1,0.975}$ denotes the 0.975 quantile of the Student-t distribution with $B-1=19$ degrees of freedom.

Analogously applying this approach to the batch mean values of $\left(Q_\ell^{X,m}\right)^2$, we define

$$\overline{R}_{\ell,b}^X := \frac{1}{n}\sum_{m\in I_b}\left(Q_\ell^{X,m}\right)^2, \qquad b=1,\dots,B, \qquad \text{and} \qquad \overline{R}_\ell^X := \frac{1}{B}\sum_{b=1}^{B}\overline{R}_{\ell,b}^X = \frac{1}{M}\sum_{m=1}^{M}\left(Q_\ell^{X,m}\right)^2,$$

with sample variance

$$S_{\ell,B,X}^2 := \frac{1}{B-1}\sum_{b=1}^{B}\left(\overline{R}_{\ell,b}^X - \overline{R}_\ell^X\right)^2.$$

Then, an approximate 95% confidence interval for the root mean square pathwise error $\left(\mathbb{E}[(Q_\ell^{X,1})^2]\right)^{1/2}$ relative to the fine-grid reference solution is given by

$$\left[\sqrt{\overline{R}_\ell^X - t_{B-1,0.975}\frac{S_{\ell,B,X}}{\sqrt{B}}}, \sqrt{\overline{R}_\ell^X + t_{B-1,0.975}\frac{S_{\ell,B,X}}{\sqrt{B}}}\right].$$

Computational cost. From a computational point of view, for a discretization with N time steps, the DIEM time recursion requires $O(N)$ operations per Monte Carlo path, apart from the cost of solving the implicit equation at the individual time steps. For the two CIR-type examples considered in this section, this equation has an explicit positive solution, and hence no iterative nonlinear solver is required. The fractional Brownian motion increments used in the numerical experiments are generated by the Davies-Harte circulant-embedding method, whose FFT-based implementation has complexity $O(N\log N)$ per path. Thus, for these examples, the simulation of the fractional noise is asymptotically more expensive than the DIEM recursion itself.

The Monte Carlo paths are mutually independent and can therefore be simulated in parallel, whereas the time recursion within each individual path is inherently sequential. This work is restricted to one-dimensional equations. In higher-dimensional fractional models, additional computational costs arise from the simulation of multidimensional fractional Brownian motion and, for general drifts, from the solution of possibly coupled nonlinear implicit equations. The development and analysis of such high-dimensional extensions are beyond the scope of this paper.

Example 5.1. Consider the following SDE:

$$\mathrm{d}Y(t) = 2K\mathrm{d}t + \sigma\sqrt{Y(t)}\mathrm{d}B^H(t), \quad t\geq 0, \quad Y(0)>0, \tag{5.1}$$

where $K>0$. By transforming $X(t)=\sqrt{Y(t)}$, Eq (5.1) can be written as

$$\mathrm{d}X(t) = \frac{K}{X(t)}\mathrm{d}t + \frac{\sigma}{2}\mathrm{d}B^H(t), \quad t\geq 0,\ X(0)=\sqrt{Y(0)}. \tag{5.2}$$

Here, $f_1(y)=2K$ and $f(x)=\frac{K}{x}$. Therefore, the conditions of Theorem 3.1 are satisfied. Consequently, Eq (5.1) has a unique pathwise solution $Y(t)$ such that $Y(t)>0$ almost surely on $[0,\infty)$. Trivially,

$$f'(x) = -\frac{K}{x^2}\leq 0, \quad f''(x)=\frac{2K}{x^3}, \quad f(x)f'(x)=\frac{-K^2}{x^3}.$$

Furthermore, Theorem 3.1 in [9], applied after the rescaling $\widetilde{X} = (2/\sigma)X$, implies that, for every $T > 0$ and $p > 0$,

$$\left(\mathbb{E}\left[\sup_{0\le t\le T}|X(t)|^p\right]\right)^{1/p} < \infty.$$

Moreover, Proposition 3.4 in [9] implies that for all $t \le \left(\frac{4K}{\sigma^2(p+1)H}\right)^{\frac{1}{2H-1}}$

$$\mathbb{E}[|X(t)|^{-p}] \le |X(0)|^{-p}. \tag{5.3}$$

Therefore, Assumptions 3.1 and 3.2 are satisfied for $t \le \left(\frac{4K}{7\sigma^2H}\right)^{\frac{1}{2H-1}}$. The DIEM scheme for Eq (5.2) is given by

$$X_{k+1} = \frac{1}{2}\left(X_k + \frac{\sigma}{2}\Delta B_k^H + \sqrt{\left(X_k + \frac{\sigma}{2}\Delta B_k^H\right)^2 + 4K\Delta}\right), \quad k = 0, 1, \ldots, \tag{5.4}$$

where $X_0 = X(0)$. Trivially, $X_k \ge 0, \ \forall\ k \ge 0$.

Proposition 5.1. *Consider the DIEM approximation* (5.4) *of* (5.2)*, and suppose that the assumptions of Theorem 4.1 are satisfied. Then we have*

$$\max_{k=1,\ldots,N}\mathbb{E}\left[\left|\frac{1}{X_k}\right|^2\right] \le C. \tag{5.5}$$

Proof. From (4.4), we get

$$e_{k+1} = e_k + K\Delta\left(\frac{1}{X(t_{k+1})} - \frac{1}{X_{k+1}}\right) + C_{k+1}^1 + C_{k+1}^2,$$

hence,

$$\frac{1}{X_{k+1}} = \frac{1}{K\Delta}\left(e_k - e_{k+1} + \frac{K\Delta}{X(t_{k+1})} + C_{k+1}^1 + C_{k+1}^2\right). \tag{5.6}$$

From Theorem 4.1, (5.3) and the estimates of I, II, III, we conclude

$$\max_{k=1,\ldots,N}\mathbb{E}\left[\left|\frac{1}{X_k}\right|^2\right] \le C. \tag{5.7}$$

For the numerical experiment, we set $K = 5$, $\sigma = 0.75$, $Y_0 = 1$ and $T = 1$ and examine the DIEM scheme for the Hurst parameters $H \in \{0.6, 0.75, 0.9\}$, which satisfy the condition $T \le (\frac{4K}{7\sigma^2H})^{\frac{1}{2H-1}}$.

To evaluate the accuracy of our scheme, we assess the Lamperti-transformed process X and the original process Y using the reference-solution procedure described above.

First, in Figure 1, we plot the RMSE of the approximation to the transformed process X and the strong error of the approximation to the original process Y. In view of Theorem 4.1 and Corollary 4.1, one expects $\widehat{\mathrm{Err}}_{X,2}(\Delta) = O(\Delta)$ and $\widehat{\mathrm{Err}}_{Y,1}(\Delta) = O(\Delta)$, which is confirmed by Figure 1.

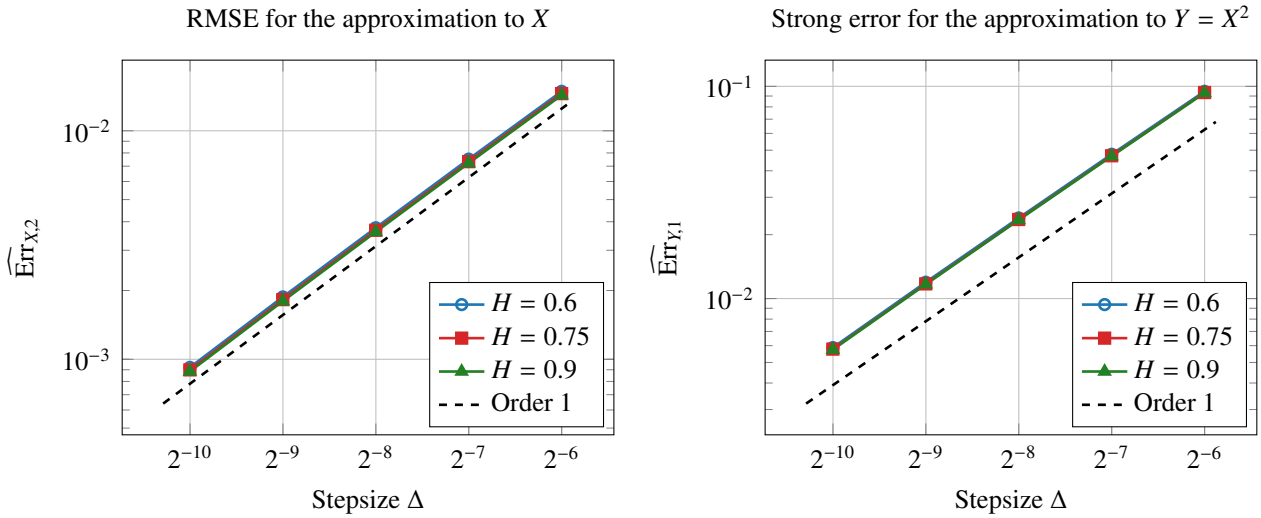

Figure 1. Monte Carlo estimates of the errors of the DIEM approximation for the transformed process (5.2) and original process (5.1) in Example 5.1.

Furthermore, Tables 1 and 2 provide the numerical RMSE and strong errors and corresponding observed convergence rates. These rates are close to the theoretical value of 1, consistently confirming the convergence order of the proposed DIEM scheme.

Moreover, for a numerical illustration of the results presented in Proposition 5.1, we plot in Figure 2 the empirical second moment

$$\widehat{\mathrm{m}}^*_{-2}(t_j) = \frac{1}{M}\sum_{m=1}^{M}\left(X^{*,m}(t_j)\right)^{-2}$$

of the inverse of the solution for Eq (5.2). For all three Hurst parameters considered, the empirical inverse second moment remains bounded over the simulated time interval, in agreement with the theoretical inverse-moment estimates.

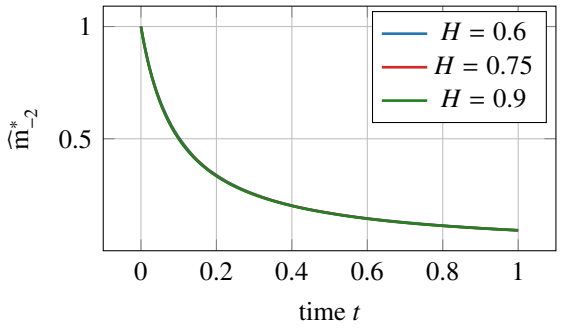

Figure 2. Monte Carlo estimates of the inverse second moment $\mathbb{E}[X(t)^{-2}] = \mathbb{E}[Y(t)^{-1}]$ for Example 5.1. The results for the different Hurst parameters coincide visually.

Table 1. RMSE for X with approximate 95% confidence intervals and observed convergence orders for Example 5.1.

H	T	Δ	$\widehat{\mathrm{Err}}_{X,2}(\Delta)$	CI lower	CI upper	$\widehat{\mathrm{p}}_{X,2}$
0.6	1	$1.563 \cdot 10^{-2}$	$1.488 \cdot 10^{-2}$	$1.481 \cdot 10^{-2}$	$1.495 \cdot 10^{-2}$	–
0.6	1	$7.813 \cdot 10^{-3}$	$7.517 \cdot 10^{-3}$	$7.480 \cdot 10^{-3}$	$7.553 \cdot 10^{-3}$	0.985
0.6	1	$3.906 \cdot 10^{-3}$	$3.763 \cdot 10^{-3}$	$3.743 \cdot 10^{-3}$	$3.783 \cdot 10^{-3}$	0.998
0.6	1	$1.953 \cdot 10^{-3}$	$1.874 \cdot 10^{-3}$	$1.866 \cdot 10^{-3}$	$1.883 \cdot 10^{-3}$	1.006
0.6	1	$9.766 \cdot 10^{-4}$	$9.213 \cdot 10^{-4}$	$9.176 \cdot 10^{-4}$	$9.251 \cdot 10^{-4}$	1.025
0.75	1	$1.563 \cdot 10^{-2}$	$1.455 \cdot 10^{-2}$	$1.447 \cdot 10^{-2}$	$1.462 \cdot 10^{-2}$	–
0.75	1	$7.813 \cdot 10^{-3}$	$7.328 \cdot 10^{-3}$	$7.291 \cdot 10^{-3}$	$7.364 \cdot 10^{-3}$	0.989
0.75	1	$3.906 \cdot 10^{-3}$	$3.670 \cdot 10^{-3}$	$3.653 \cdot 10^{-3}$	$3.687 \cdot 10^{-3}$	0.998
0.75	1	$1.953 \cdot 10^{-3}$	$1.825 \cdot 10^{-3}$	$1.816 \cdot 10^{-3}$	$1.834 \cdot 10^{-3}$	1.008
0.75	1	$9.766 \cdot 10^{-4}$	$8.989 \cdot 10^{-4}$	$8.947 \cdot 10^{-4}$	$9.032 \cdot 10^{-4}$	1.021
0.9	1	$1.563 \cdot 10^{-2}$	$1.432 \cdot 10^{-2}$	$1.427 \cdot 10^{-2}$	$1.438 \cdot 10^{-2}$	–
0.9	1	$7.813 \cdot 10^{-3}$	$7.214 \cdot 10^{-3}$	$7.187 \cdot 10^{-3}$	$7.241 \cdot 10^{-3}$	0.989
0.9	1	$3.906 \cdot 10^{-3}$	$3.611 \cdot 10^{-3}$	$3.597 \cdot 10^{-3}$	$3.624 \cdot 10^{-3}$	0.999
0.9	1	$1.953 \cdot 10^{-3}$	$1.795 \cdot 10^{-3}$	$1.789 \cdot 10^{-3}$	$1.802 \cdot 10^{-3}$	1.008
0.9	1	$9.766 \cdot 10^{-4}$	$8.846 \cdot 10^{-4}$	$8.812 \cdot 10^{-4}$	$8.880 \cdot 10^{-4}$	1.021

Table 2. Strong error for $Y = X^2$ with approximate 95% confidence intervals and observed convergence orders for Example 5.1.

H	T	Δ	$\widehat{\mathrm{Err}}_{Y,1}(\Delta)$	CI lower	CI upper	$\widehat{\mathrm{p}}_{Y,1}$
0.6	1	$1.563 \cdot 10^{-2}$	$9.467 \cdot 10^{-2}$	$9.379 \cdot 10^{-2}$	$9.555 \cdot 10^{-2}$	–
0.6	1	$7.813 \cdot 10^{-3}$	$4.783 \cdot 10^{-2}$	$4.738 \cdot 10^{-2}$	$4.828 \cdot 10^{-2}$	0.985
0.6	1	$3.906 \cdot 10^{-3}$	$2.397 \cdot 10^{-2}$	$2.371 \cdot 10^{-2}$	$2.423 \cdot 10^{-2}$	0.997
0.6	1	$1.953 \cdot 10^{-3}$	$1.194 \cdot 10^{-2}$	$1.182 \cdot 10^{-2}$	$1.205 \cdot 10^{-2}$	1.006
0.6	1	$9.766 \cdot 10^{-4}$	$5.872 \cdot 10^{-3}$	$5.816 \cdot 10^{-3}$	$5.929 \cdot 10^{-3}$	1.023
0.75	1	$1.563 \cdot 10^{-2}$	$9.347 \cdot 10^{-2}$	$9.245 \cdot 10^{-2}$	$9.449 \cdot 10^{-2}$	–
0.75	1	$7.813 \cdot 10^{-3}$	$4.707 \cdot 10^{-2}$	$4.656 \cdot 10^{-2}$	$4.758 \cdot 10^{-2}$	0.99
0.75	1	$3.906 \cdot 10^{-3}$	$2.358 \cdot 10^{-2}$	$2.333 \cdot 10^{-2}$	$2.383 \cdot 10^{-2}$	0.998
0.75	1	$1.953 \cdot 10^{-3}$	$1.173 \cdot 10^{-2}$	$1.160 \cdot 10^{-2}$	$1.185 \cdot 10^{-2}$	1.008
0.75	1	$9.766 \cdot 10^{-4}$	$5.777 \cdot 10^{-3}$	$5.716 \cdot 10^{-3}$	$5.838 \cdot 10^{-3}$	1.021
0.9	1	$1.563 \cdot 10^{-2}$	$9.309 \cdot 10^{-2}$	$9.225 \cdot 10^{-2}$	$9.394 \cdot 10^{-2}$	–
0.9	1	$7.813 \cdot 10^{-3}$	$4.688 \cdot 10^{-2}$	$4.646 \cdot 10^{-2}$	$4.730 \cdot 10^{-2}$	0.99
0.9	1	$3.906 \cdot 10^{-3}$	$2.346 \cdot 10^{-2}$	$2.325 \cdot 10^{-2}$	$2.367 \cdot 10^{-2}$	0.999
0.9	1	$1.953 \cdot 10^{-3}$	$1.166 \cdot 10^{-2}$	$1.156 \cdot 10^{-2}$	$1.177 \cdot 10^{-2}$	1.008
0.9	1	$9.766 \cdot 10^{-4}$	$5.746 \cdot 10^{-3}$	$5.694 \cdot 10^{-3}$	$5.798 \cdot 10^{-3}$	1.021

Example 5.2. Consider the following CIR model:

$$\mathrm{d}Y(t) = K(\theta - Y(t))\mathrm{d}t + \sigma\sqrt{Y(t)}\mathrm{d}B^H(t), \quad t \geq 0, \quad Y(0) > 0, \tag{5.8}$$

where $K, \theta, \sigma > 0$. From (3.2), by defining $X(t) = \sqrt{Y(t)}$, Eq (5.8) can be written as

$$\mathrm{d}X(t) = \frac{K}{2}\left(\frac{\theta}{X(t)} - X(t)\right)\mathrm{d}t + \frac{\sigma}{2}\mathrm{d}B^H(t), \quad t \geq 0, \;\; X(0) = \sqrt{Y(0)}. \tag{5.9}$$

By Proposition 3.1 in [24], for every $T > 0$ and $p \geq 1$, there exists a unique solution $X(t)$ of Eq (5.9) satisfying

$$\left(\mathbb{E}\left[\sup_{0\leq t\leq T}|X(t)|^p\right]\right)^{\frac{1}{p}} < \infty, \tag{5.10}$$

and if, in addition,

$$K\theta\exp\left(\frac{Ks}{2}\right) \geq (p+1)\int_0^s \frac{\sigma^2}{2}\exp\left(\frac{K\varsigma}{2}\right)\varrho(\varsigma, s)d\varsigma, \;\; 0 \leq s \leq T,$$

holds, then

$$\sup_{0\leq t\leq T}\left(\mathbb{E}\left[|X(t)^{-1}|^p\right]\right)^{\frac{1}{p}} < \infty.$$

For this equation,

$$f_1(y) = K\theta - Ky, \; f(x) = \frac{K}{2}\left(\frac{\theta}{x} - x\right),$$

and hence

$$f'(x) = -\frac{K}{2}\left(\theta x^{-2} + 1\right) < 0, \qquad f'(x)f(x) = -\frac{K^2}{4}\left(\theta^2 x^{-3} - x\right), \qquad f''(x) = K\theta x^{-3}.$$

Hence, Assumption 3.1 is fulfilled, and Assumption 3.2 holds under the condition that

$$K\theta\exp\left(\frac{Ks}{2}\right) \geq 7\int_0^s \frac{\sigma^2}{2}\exp\left(\frac{K\varsigma}{2}\right)\varrho(\varsigma, s)d\varsigma, \;\; 0 \leq s \leq T. \tag{5.11}$$

Together with Remarks 3.3 and 3.4, this shows that Assumptions 3.1–3.4 are satisfied for the transformed fractional CIR equation under (5.11). Consequently, Theorem 4.1 applies.

The numerical scheme (3.5) for SDE (5.9) is given by

$$X_{k+1} = X_k + \frac{K}{2}\left(\frac{\theta}{X_{k+1}} - X_{k+1}\right)\Delta + \frac{\sigma}{2}\Delta B_k^H, \quad k = 0, 1, ..., N-1, \tag{5.12}$$

with $X_0 = X(0)$. Note that the unique solution to (5.12) is given by

$$X_{k+1} = \frac{1}{2 + K\Delta}\left(X_k + \frac{\sigma}{2}\Delta B_k^H + \sqrt{\left(X_k + \frac{\sigma}{2}\Delta B_k^H\right)^2 + 2K\theta\Delta(1 + \frac{K\Delta}{2})}\right), \tag{5.13}$$

which trivially implies $X_k \geq 0, \; k > 0$. We can also demonstrate that the second moment of the inverse numerical solution remains bounded, analogous to the observations made in Proposition 5.1. For our numerical experiment, we use the CIR parameters reported by Chan et al. [30] as an empirically motivated benchmark. Using 306 monthly observations of the annualized one-month U.S. Treasury bill yield from June 1964 to December 1989, they obtained the parameter estimates

$$\theta = 0.0808, \qquad \sigma = \sqrt{0.0073} \approx 0.0854, \qquad K = 0.2339.$$

We initialize the process at its mean-reversion level,

$$Y_0 = \theta = 0.0808, \qquad X_0 = \sqrt{\theta}.$$

Thus, the experiment should not be interpreted as a calibration of the fractional CIR model.

In the following, we compute the numerical errors using the same reference-solution procedure described at the beginning of this section.

Figure 3 shows the RMSE of the numerical approximation to the transformed process (5.9) and the strong error of the numerical approximation to the original process (5.8) for different step sizes. We consider $H = 0.6$ and 0.75 with $T = 1$, and $H = 0.9$ with $T = 0.8$. The numerical results confirm the findings presented in Theorem 4.1 and Corollary 4.1.

Furthermore, Figure 4 graphically illustrates the bounded behavior observed for the second moment of the inverse solution of Eq (5.9).

We also verify that the parameter choices used above satisfy the condition given in (5.11). Using (2.3), (5.11) can equivalently be written as

$$K\theta \geq \frac{7\sigma^2}{2} H(2H-1) \int_0^s \exp\left(-\frac{Ku}{2}\right) u^{2H-2}\, du.$$

The right-hand side is increasing in s, so it is sufficient to verify the inequality at $s = T$. For the parameter sets used in the numerical experiments, the ratios of the left-hand side to the right-hand side at $s = T$ are approximately

$$1.257, \qquad 1.025, \qquad 1.024$$

for

$$(H, T) = (0.6, 1), \qquad (0.75, 1), \qquad (0.9, 0.8),$$

respectively. Hence, the required condition is satisfied in all three cases.

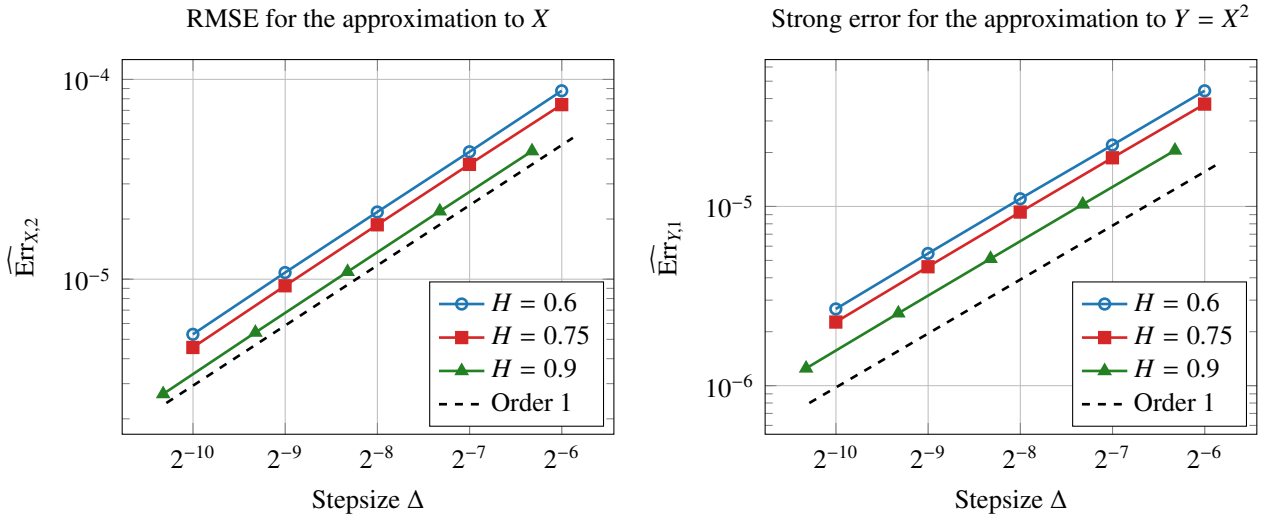

Figure 3. Monte Carlo estimates of the errors of the DIEM approximation for the transformed process (5.9) and original process (5.8) in Example 5.2.

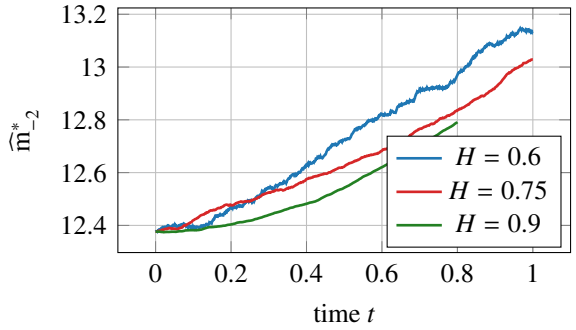

Figure 4. Monte Carlo estimates of the inverse second moment $\mathbb{E}[X(t)^{-2}] = \mathbb{E}[Y(t)^{-1}]$ for Example 5.2.

Comparison with existing numerical methods. Tables 3 and 4 compare the DIEM method with the positivity-preserving truncated Euler-Maruyama scheme of Gao et al. [22]. In the notation of this paper, define $\pi_\Delta(x) = \max\{L\Delta^\alpha, x\}$, and let $U_0 = x_0$. We choose $\alpha = \frac{1}{4}$, $L = x_0 = \sqrt{\theta}$, which satisfies the admissibility conditions $0 < \alpha \le \frac{1}{4}$ and $0 < L \le x_0$ in [22]. The method is given by

$$U_{k+1} = U_k + \frac{K}{2}\left(\frac{\theta}{\pi_\Delta(U_k)} - \pi_\Delta(U_k)\right)\Delta + \frac{\sigma}{2}\Delta B_k^H,$$

with the positive approximation

$$X_k^{\mathrm{G}} = \pi_\Delta(U_k), \qquad Y_k^{\mathrm{G}} = (X_k^{\mathrm{G}})^2.$$

At each level ℓ, the DIEM and truncated Euler-Maruyama approximations are driven by the same aggregated fractional Brownian motion increments and are compared with the same fine-grid reference solution with $N_* = 2^{19}$ time steps.

Table 3. Comparison of the RMSE for the transformed process X in Example 5.2. The errors are based on $M = 1000$ Monte Carlo paths and the common reference discretization $N_* = 2^{19}$. The intervals are approximate 95% confidence intervals obtained from $B = 20$ batches of 50 paths. The observed rate in each row is computed from that row and the preceding coarser discretization.

H	Δ	$\widehat{\mathrm{Err}}_{X,2}(\Delta)$ DIEM	DIEM CI lower	DIEM CI upper	$\widehat{\mathrm{p}}_{X,2}$ DIEM	$\widehat{\mathrm{Err}}_{X,2}(\Delta)$ Gao	Gao CI lower	Gao CI upper	$\widehat{\mathrm{p}}_{X,2}$ Gao
0.6	$1.563 \cdot 10^{-2}$	$8.726 \cdot 10^{-5}$	$8.367 \cdot 10^{-5}$	$9.071 \cdot 10^{-5}$	–	$8.723 \cdot 10^{-5}$	$8.439 \cdot 10^{-5}$	$8.998 \cdot 10^{-5}$	–
0.6	$7.813 \cdot 10^{-3}$	$4.395 \cdot 10^{-5}$	$4.212 \cdot 10^{-5}$	$4.570 \cdot 10^{-5}$	0.99	$4.370 \cdot 10^{-5}$	$4.237 \cdot 10^{-5}$	$4.499 \cdot 10^{-5}$	0.997
0.6	$3.906 \cdot 10^{-3}$	$2.204 \cdot 10^{-5}$	$2.117 \cdot 10^{-5}$	$2.287 \cdot 10^{-5}$	0.996	$2.173 \cdot 10^{-5}$	$2.100 \cdot 10^{-5}$	$2.244 \cdot 10^{-5}$	1.008
0.6	$1.953 \cdot 10^{-3}$	$1.100 \cdot 10^{-5}$	$1.061 \cdot 10^{-5}$	$1.137 \cdot 10^{-5}$	1.003	$1.088 \cdot 10^{-5}$	$1.049 \cdot 10^{-5}$	$1.126 \cdot 10^{-5}$	0.998
0.6	$9.766 \cdot 10^{-4}$	$5.443 \cdot 10^{-6}$	$5.239 \cdot 10^{-6}$	$5.638 \cdot 10^{-6}$	1.015	$5.456 \cdot 10^{-6}$	$5.265 \cdot 10^{-6}$	$5.641 \cdot 10^{-6}$	0.996
0.75	$1.563 \cdot 10^{-2}$	$7.344 \cdot 10^{-5}$	$7.087 \cdot 10^{-5}$	$7.592 \cdot 10^{-5}$	–	$7.418 \cdot 10^{-5}$	$7.164 \cdot 10^{-5}$	$7.663 \cdot 10^{-5}$	–
0.75	$7.813 \cdot 10^{-3}$	$3.695 \cdot 10^{-5}$	$3.567 \cdot 10^{-5}$	$3.818 \cdot 10^{-5}$	0.991	$3.696 \cdot 10^{-5}$	$3.566 \cdot 10^{-5}$	$3.821 \cdot 10^{-5}$	1.005
0.75	$3.906 \cdot 10^{-3}$	$1.847 \cdot 10^{-5}$	$1.784 \cdot 10^{-5}$	$1.909 \cdot 10^{-5}$	1	$1.850 \cdot 10^{-5}$	$1.785 \cdot 10^{-5}$	$1.912 \cdot 10^{-5}$	0.999
0.75	$1.953 \cdot 10^{-3}$	$9.224 \cdot 10^{-6}$	$8.907 \cdot 10^{-6}$	$9.530 \cdot 10^{-6}$	1.002	$9.256 \cdot 10^{-6}$	$8.939 \cdot 10^{-6}$	$9.562 \cdot 10^{-6}$	0.999
0.75	$9.766 \cdot 10^{-4}$	$4.615 \cdot 10^{-6}$	$4.457 \cdot 10^{-6}$	$4.768 \cdot 10^{-6}$	0.999	$4.620 \cdot 10^{-6}$	$4.460 \cdot 10^{-6}$	$4.774 \cdot 10^{-6}$	1.003
0.9	$1.250 \cdot 10^{-2}$	$4.551 \cdot 10^{-5}$	$4.329 \cdot 10^{-5}$	$4.762 \cdot 10^{-5}$	–	$4.566 \cdot 10^{-5}$	$4.341 \cdot 10^{-5}$	$4.780 \cdot 10^{-5}$	–
0.9	$6.250 \cdot 10^{-3}$	$2.278 \cdot 10^{-5}$	$2.167 \cdot 10^{-5}$	$2.383 \cdot 10^{-5}$	0.999	$2.282 \cdot 10^{-5}$	$2.169 \cdot 10^{-5}$	$2.389 \cdot 10^{-5}$	1.001
0.9	$3.125 \cdot 10^{-3}$	$1.139 \cdot 10^{-5}$	$1.084 \cdot 10^{-5}$	$1.191 \cdot 10^{-5}$	1	$1.141 \cdot 10^{-5}$	$1.085 \cdot 10^{-5}$	$1.195 \cdot 10^{-5}$	1
0.9	$1.563 \cdot 10^{-3}$	$5.694 \cdot 10^{-6}$	$5.416 \cdot 10^{-6}$	$5.958 \cdot 10^{-6}$	1	$5.706 \cdot 10^{-6}$	$5.427 \cdot 10^{-6}$	$5.972 \cdot 10^{-6}$	1
0.9	$7.813 \cdot 10^{-4}$	$2.845 \cdot 10^{-6}$	$2.707 \cdot 10^{-6}$	$2.977 \cdot 10^{-6}$	1.001	$2.855 \cdot 10^{-6}$	$2.715 \cdot 10^{-6}$	$2.988 \cdot 10^{-6}$	0.999

Table 4. Comparison of the empirical L^1 error for the original process $Y = X^2$ in Example 5.2. The errors are based on $M = 1000$ Monte Carlo paths and the common reference discretization $N_* = 2^{19}$. The intervals are approximate 95% confidence intervals obtained from $B = 20$ batches of 50 paths. The observed rate in each row is computed from that row and the preceding coarser discretization.

H	Δ	$\widehat{\mathrm{Err}}_{Y,1}(\Delta)$ DIEM L^1	DIEM CI lower	DIEM CI upper	$\widehat{\mathrm{p}}_{Y,1}$ DIEM	$\widehat{\mathrm{Err}}_{Y,1}(\Delta)$ Gao L^1	Gao CI lower	Gao CI upper	$\widehat{\mathrm{p}}_{Y,1}$ Gao
0.6	$1.563 \cdot 10^{-2}$	$4.355 \cdot 10^{-5}$	$4.225 \cdot 10^{-5}$	$4.485 \cdot 10^{-5}$	–	$4.365 \cdot 10^{-5}$	$4.258 \cdot 10^{-5}$	$4.471 \cdot 10^{-5}$	–
0.6	$7.813 \cdot 10^{-3}$	$2.190 \cdot 10^{-5}$	$2.118 \cdot 10^{-5}$	$2.263 \cdot 10^{-5}$	0.992	$2.190 \cdot 10^{-5}$	$2.139 \cdot 10^{-5}$	$2.241 \cdot 10^{-5}$	0.995
0.6	$3.906 \cdot 10^{-3}$	$1.102 \cdot 10^{-5}$	$1.067 \cdot 10^{-5}$	$1.138 \cdot 10^{-5}$	0.991	$1.089 \cdot 10^{-5}$	$1.060 \cdot 10^{-5}$	$1.118 \cdot 10^{-5}$	1.008
0.6	$1.953 \cdot 10^{-3}$	$5.507 \cdot 10^{-6}$	$5.350 \cdot 10^{-6}$	$5.664 \cdot 10^{-6}$	1.001	$5.436 \cdot 10^{-6}$	$5.291 \cdot 10^{-6}$	$5.581 \cdot 10^{-6}$	1.003
0.6	$9.766 \cdot 10^{-4}$	$2.732 \cdot 10^{-6}$	$2.660 \cdot 10^{-6}$	$2.805 \cdot 10^{-6}$	1.011	$2.731 \cdot 10^{-6}$	$2.646 \cdot 10^{-6}$	$2.817 \cdot 10^{-6}$	0.993
0.75	$1.563 \cdot 10^{-2}$	$3.681 \cdot 10^{-5}$	$3.580 \cdot 10^{-5}$	$3.782 \cdot 10^{-5}$	–	$3.713 \cdot 10^{-5}$	$3.603 \cdot 10^{-5}$	$3.823 \cdot 10^{-5}$	–
0.75	$7.813 \cdot 10^{-3}$	$1.854 \cdot 10^{-5}$	$1.802 \cdot 10^{-5}$	$1.905 \cdot 10^{-5}$	0.989	$1.850 \cdot 10^{-5}$	$1.794 \cdot 10^{-5}$	$1.905 \cdot 10^{-5}$	1.005
0.75	$3.906 \cdot 10^{-3}$	$9.271 \cdot 10^{-6}$	$8.999 \cdot 10^{-6}$	$9.542 \cdot 10^{-6}$	1	$9.267 \cdot 10^{-6}$	$9.000 \cdot 10^{-6}$	$9.533 \cdot 10^{-6}$	0.997
0.75	$1.953 \cdot 10^{-3}$	$4.623 \cdot 10^{-6}$	$4.489 \cdot 10^{-6}$	$4.757 \cdot 10^{-6}$	1.004	$4.642 \cdot 10^{-6}$	$4.509 \cdot 10^{-6}$	$4.775 \cdot 10^{-6}$	0.997
0.75	$9.766 \cdot 10^{-4}$	$2.314 \cdot 10^{-6}$	$2.247 \cdot 10^{-6}$	$2.381 \cdot 10^{-6}$	0.999	$2.317 \cdot 10^{-6}$	$2.251 \cdot 10^{-6}$	$2.383 \cdot 10^{-6}$	1.003
0.9	$1.250 \cdot 10^{-2}$	$2.135 \cdot 10^{-5}$	$2.030 \cdot 10^{-5}$	$2.239 \cdot 10^{-5}$	–	$2.144 \cdot 10^{-5}$	$2.038 \cdot 10^{-5}$	$2.249 \cdot 10^{-5}$	–
0.9	$6.250 \cdot 10^{-3}$	$1.070 \cdot 10^{-5}$	$1.018 \cdot 10^{-5}$	$1.122 \cdot 10^{-5}$	0.997	$1.071 \cdot 10^{-5}$	$1.017 \cdot 10^{-5}$	$1.124 \cdot 10^{-5}$	1.002
0.9	$3.125 \cdot 10^{-3}$	$5.349 \cdot 10^{-6}$	$5.085 \cdot 10^{-6}$	$5.612 \cdot 10^{-6}$	1	$5.355 \cdot 10^{-6}$	$5.091 \cdot 10^{-6}$	$5.618 \cdot 10^{-6}$	1
0.9	$1.563 \cdot 10^{-3}$	$2.674 \cdot 10^{-6}$	$2.543 \cdot 10^{-6}$	$2.805 \cdot 10^{-6}$	1	$2.678 \cdot 10^{-6}$	$2.546 \cdot 10^{-6}$	$2.811 \cdot 10^{-6}$	0.999
0.9	$7.813 \cdot 10^{-4}$	$1.336 \cdot 10^{-6}$	$1.271 \cdot 10^{-6}$	$1.401 \cdot 10^{-6}$	1.001	$1.341 \cdot 10^{-6}$	$1.274 \cdot 10^{-6}$	$1.407 \cdot 10^{-6}$	0.998

For the parameter sets considered here, the two methods yield very similar errors, and the observed convergence rates are close to one for the transformed process X and the original process Y. This numerical observation should be distinguished from the available theoretical convergence guarantees. Gao et al. [22] established strong convergence of order H for their truncated Euler-Maruyama scheme, whereas the DIEM approximation converges with strong order one under the assumptions of Corollary 4.1. Thus, although the two methods show very similar errors in this CIR experiment, their available theoretical convergence results are different.

It is also noteworthy that the truncation in the method of Gao et al. was not activated for any of the simulated paths and step sizes in this experiment, and none of the corresponding untruncated Euler updates became negative. Thus, for the present parameter regime, the truncated method effectively behaves like its underlying explicit Euler discretization, which could explain why its observed convergence behavior is substantially better than the general order-H bound might suggest.

Financial path functional. To illustrate how the pathwise approximation relates to a financially relevant quantity, we also consider the functional

$$D(0,T) = \mathbb{E}\left(e^{-\int_0^T Y_s ds}\right),$$

which depends on the integrated short rate.

For the mth numerical path on the grid with step size Δ_ℓ, we approximate the time integral by the trapezoidal rule and define

$$\mathcal{D}_\ell^{(m)}(T) := e^{-\Delta_\ell\left(\frac{1}{2}Y_{\ell,0}^{(m)} + \sum_{k=1}^{N_\ell - 1} Y_{\ell,k}^{(m)} + \frac{1}{2}Y_{\ell,N_\ell}^{(m)}\right)}.$$

The corresponding Monte Carlo estimator of the expected discount factor is

$$\widehat{D}_\ell(0,T) := \frac{1}{M}\sum_{m=1}^{M} \mathcal{D}_\ell^{(m)}(T).$$

Analogously, using the fine-grid reference approximation, we obtain $\mathcal{D}_*^{(m)}(T)$ and

$$\widehat{D}_*(0,T) := \frac{1}{M}\sum_{m=1}^{M} \mathcal{D}_*^{(m)}(T).$$

Since the coarse and reference approximations for each Monte Carlo path are generated from the same realization of the fractional Brownian motion, we estimate the weak discretization bias using the paired differences

$$Z_\ell^{(m)} := \mathcal{D}_\ell^{(m)}(T) - \mathcal{D}_*^{(m)}(T).$$

Thus,

$$\widehat{b}_D(\Delta_\ell) := \frac{1}{M}\sum_{m=1}^{M} Z_\ell^{(m)} = \widehat{D}_\ell(0,T) - \widehat{D}_*(0,T),$$

and we use

$$\widehat{\mathrm{Err}}_D(\Delta_\ell) := \left|\widehat{b}_D(\Delta_\ell)\right|$$

as an estimate of the absolute weak discretization bias relative to the fine-grid reference solution.

Since the weak error is substantially smaller than the pathwise strong errors considered above, we use $M = 100\,000$ independent Monte Carlo paths for this experiment. The corresponding observed convergence orders, as well as the 95% confidence intervals for the signed bias $\mathbb{E}[Z_\ell^{(1)}]$, are then calculated as described above, using 20 independent batches of 5000 paths each.

Table 5 reports the numerical approximations of the expected discount factor, the estimated absolute weak errors, the confidence intervals for the signed biases, and the corresponding observed convergence orders, which are consistent with first-order convergence. Since we do not specify a risk-neutral pricing measure for the fractional model, $D(0,T)$ should not be interpreted as an arbitrage-free zero-coupon bond price but rather as a financially relevant discount factor.

Finally, Figure 5 shows 10 simulated interest-rate paths for each of the three Hurst parameters, generated with the fine-grid DIEM reference discretization.

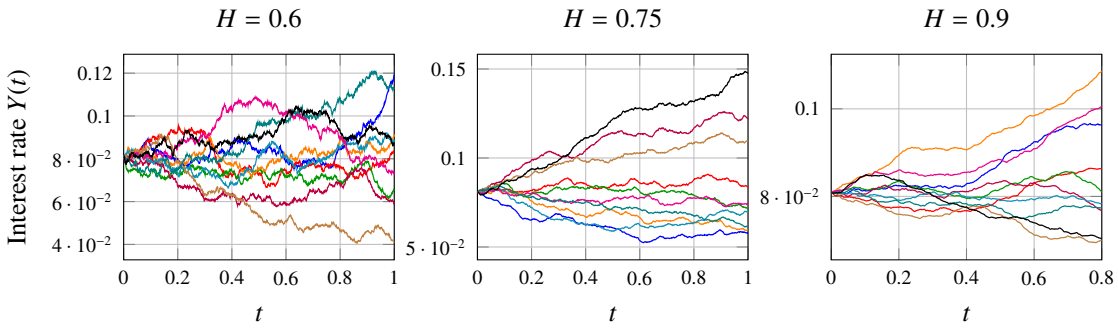

Figure 5. Ten simulated sample paths of the fractional CIR short-rate process for each of the three Hurst parameters considered in Example 5.2. The paths are generated using the fine-grid DIEM reference discretization.

Table 5. Convergence of the numerical approximation $\widehat{D}_\ell(0,T)$ of the expected discount factor in Example 5.2. The estimated weak error is $\widehat{\mathrm{Err}}_D(\Delta_\ell) = |\widehat{b}_D(\Delta_\ell)|$. The reported approximate 95% confidence interval refers to the signed bias $\mathbb{E}[Z_\ell^{(1)}]$, estimated by $\widehat{b}_D(\Delta_\ell) = \widehat{D}_\ell(0,T) - \widehat{D}_*(0,T)$.

H	T	Δ	$\widehat{D}_\ell(0,T)$	$\widehat{\mathrm{Err}}_D(\Delta)$	CI lower	CI upper	$\widehat{p}_D$
0.6	1	$1.563 \cdot 10^{-2}$	0.921762	$8.995 \cdot 10^{-7}$	$6.550 \cdot 10^{-7}$	$1.144 \cdot 10^{-6}$	–
0.6	1	$7.813 \cdot 10^{-3}$	0.921761	$5.470 \cdot 10^{-7}$	$4.214 \cdot 10^{-7}$	$6.727 \cdot 10^{-7}$	0.718
0.6	1	$3.906 \cdot 10^{-3}$	0.921761	$2.507 \cdot 10^{-7}$	$1.925 \cdot 10^{-7}$	$3.090 \cdot 10^{-7}$	1.125
0.6	1	$1.953 \cdot 10^{-3}$	0.921761	$1.545 \cdot 10^{-7}$	$1.238 \cdot 10^{-7}$	$1.852 \cdot 10^{-7}$	0.699
0.6	1	$9.766 \cdot 10^{-4}$	0.921761	$6.726 \cdot 10^{-8}$	$4.937 \cdot 10^{-8}$	$8.515 \cdot 10^{-8}$	1.2
0.75	1	$1.563 \cdot 10^{-2}$	0.921789	$9.821 \cdot 10^{-7}$	$7.901 \cdot 10^{-7}$	$1.174 \cdot 10^{-6}$	–
0.75	1	$7.813 \cdot 10^{-3}$	0.921789	$4.944 \cdot 10^{-7}$	$4.017 \cdot 10^{-7}$	$5.870 \cdot 10^{-7}$	0.99
0.75	1	$3.906 \cdot 10^{-3}$	0.921789	$2.467 \cdot 10^{-7}$	$1.981 \cdot 10^{-7}$	$2.954 \cdot 10^{-7}$	1.003
0.75	1	$1.953 \cdot 10^{-3}$	0.921789	$1.316 \cdot 10^{-7}$	$1.088 \cdot 10^{-7}$	$1.544 \cdot 10^{-7}$	0.907
0.75	1	$9.766 \cdot 10^{-4}$	0.921789	$6.278 \cdot 10^{-8}$	$5.308 \cdot 10^{-8}$	$7.247 \cdot 10^{-8}$	1.068
0.9	0.8	$1.250 \cdot 10^{-2}$	0.937159	$2.770 \cdot 10^{-7}$	$2.149 \cdot 10^{-7}$	$3.391 \cdot 10^{-7}$	–
0.9	0.8	$6.250 \cdot 10^{-3}$	0.937159	$1.546 \cdot 10^{-7}$	$1.236 \cdot 10^{-7}$	$1.855 \cdot 10^{-7}$	0.841
0.9	0.8	$3.125 \cdot 10^{-3}$	0.937159	$7.935 \cdot 10^{-8}$	$6.426 \cdot 10^{-8}$	$9.444 \cdot 10^{-8}$	0.962
0.9	0.8	$1.563 \cdot 10^{-3}$	0.937159	$4.062 \cdot 10^{-8}$	$3.321 \cdot 10^{-8}$	$4.803 \cdot 10^{-8}$	0.966
0.9	0.8	$7.813 \cdot 10^{-4}$	0.937159	$1.979 \cdot 10^{-8}$	$1.623 \cdot 10^{-8}$	$2.335 \cdot 10^{-8}$	1.037

Example 5.3. A classical 3/2 stochastic-volatility specification, related to the model discussed by Heston [31], is given in the fractional setting by

$$\begin{aligned} &\mathrm{d}Y(t) = c_1 Y(t)(c_2 - Y(t))\mathrm{d}t + c_3 Y(t)^{3/2}\mathrm{d}B^H(t), \qquad t \in [0,T], \\ &Y(0) = y_0 > 0, \end{aligned} \tag{5.14}$$

where the parameters satisfy $c_1, c_2, c_3 > 0$. Notice that (5.14) is not of the square-root form (3.1). However, its reciprocal is a fractional CIR process. Indeed, define

$$R(t) := Y(t)^{-1} \qquad \text{and} \qquad \widetilde{B}^H(t) := -B^H(t).$$

Since $\widetilde{B}^H$ is again a fractional Brownian motion with Hurst parameter H, the Young chain rule gives

$$\begin{aligned} \mathrm{d}R(t) &= c_1(1 - c_2 R(t))\mathrm{d}t + c_3 \sqrt{R(t)}\ \mathrm{d}\widetilde{B}^H(t) \\ &= K(\theta - R(t))\mathrm{d}t + \sigma\sqrt{R(t)}\ \mathrm{d}\widetilde{B}^H(t), \end{aligned} \tag{5.15}$$

where

$$K = c_1 c_2, \qquad \theta = \frac{1}{c_2}, \qquad \sigma = c_3. \tag{5.16}$$

Thus, R is of exactly the same fractional CIR form as the process in (5.8).

Equivalently, with

$$X(t) := \sqrt{R(t)} = Y(t)^{-1/2},$$

the transformed equation becomes

$$\begin{aligned} \mathrm{d}X(t) &= \frac{K}{2}\left(\frac{\theta}{X(t)} - X(t)\right)\mathrm{d}t + \frac{\sigma}{2}\,\mathrm{d}\,\widetilde{B}^H(t), \qquad t \in [0,T], \\ X(0) &= y_0^{-1/2}. \end{aligned} \tag{5.17}$$

Consequently, the DIEM approximation X_k is given by the same positive drift-implicit recursion as in (5.12), with the parameters in (5.16) and with increments of $\widetilde{B}^H$.

An approximation to the original 3/2 process is then obtained by the inverse-square transformation

$$Y_k := X_k^{-2}.$$

Unlike the transformation $Y = X^2$ considered in Corollary 4.1, the map $x \mapsto x^{-2}$ is singular at the origin. Therefore, convergence of X_k alone is not sufficient to obtain the same result for Y_k; suitable inverse-moment bounds for both the exact and numerical transformed solutions are required.

Corollary 5.1. *(Strong convergence for the fractional Heston-3/2 model) Consider the setting of Example 5.3, and let X_k be the positive DIEM approximation to* (5.17)*. Suppose that*

$$K\theta \exp\left(\frac{Ks}{2}\right) \geq 19 \int_0^s \frac{\sigma^2}{2} \exp\left(\frac{K\varsigma}{2}\right) \varrho(\varsigma, s)\,\mathrm{d}\varsigma, \qquad 0 \leq s \leq T. \tag{5.18}$$

Define

$$Y_k := X_k^{-2}.$$

Then there exists a constant $C_T > 0$, independent of the step size Δ, such that, for all sufficiently small Δ,

$$\max_{0\leq k\leq N} \mathbb{E}\left[|Y(t_k) - Y_k|\right] \leq C_T \Delta. \tag{5.19}$$

Hence, the approximation of the original fractional Heston-3/2 process converges strongly with order one in $L^1(\Omega)$, uniformly at the grid points.

Proof. By (5.16) and (5.17), the transformed process $X = Y^{-1/2}$ satisfies, up to replacing B^H by the fractional Brownian motion $\widetilde{B}^H$, exactly the transformed fractional CIR equation (5.9) considered in Example 5.2. Likewise, its DIEM approximation X_k is given by the same recursion as (5.12), with increments of $\widetilde{B}^H$.

Since the integrand in (5.11) is nonnegative, condition (5.18) implies (5.11). Hence, by the verification in Example 5.2, all assumptions of Theorem 4.1 are satisfied, and therefore

$$\left(\mathbb{E}\left[\max_{0\leq k\leq N} |X(t_k) - X_k|^2\right]\right)^{1/2} \leq C\Delta. \tag{5.20}$$

It remains to control the inverse-square transformation. Condition (5.18) is the inverse-moment condition in Theorem 4.1 of Hong et al. [24] with $p = 6$. Propositions 3.1 and 4.1 of Hong et al. [24] therefore imply, respectively,

$$\sup_{0\leq t\leq T} \mathbb{E}\left[X(t)^{-6}\right] < \infty \qquad \text{and} \qquad \sup_{\Delta} \max_{0\leq k\leq N} \mathbb{E}\left[X_k^{-6}\right] < \infty, \tag{5.21}$$

where the supremum over Δ is understood over sufficiently small step sizes.

For arbitrary $a, b > 0$,

$$|a^{-2} - b^{-2}| = |a - b|\frac{a+b}{a^2b^2} = |a - b|\left(a^{-1}b^{-2} + a^{-2}b^{-1}\right).$$

Young's inequality gives

$$a^{-1}b^{-2} \le \frac{1}{3}a^{-3} + \frac{2}{3}b^{-3} \qquad \text{and} \qquad a^{-2}b^{-1} \le \frac{2}{3}a^{-3} + \frac{1}{3}b^{-3}.$$

Consequently,

$$|a^{-2} - b^{-2}| \le |a - b|\left(a^{-3} + b^{-3}\right). \tag{5.22}$$

Applying (5.22) with $a = X(t_k)$ and $b = X_k$, and using the Cauchy-Schwarz and the triangle inequality, we obtain

$$\mathbb{E}\left[|Y(t_k) - Y_k|\right] = \mathbb{E}\left[|X(t_k)^{-2} - X_k^{-2}|\right] \le \left(\mathbb{E}|X(t_k) - X_k|^2\right)^{1/2} \times \left[\left(\mathbb{E}X(t_k)^{-6}\right)^{1/2} + \left(\mathbb{E}X_k^{-6}\right)^{1/2}\right].$$

By (5.20), the first factor is bounded by $C\Delta$, uniformly in k. By (5.21), the second factor is bounded uniformly in k and Δ. Therefore,

$$\max_{0\le k\le N} \mathbb{E}\left[|Y(t_k) - Y_k|\right] \le C_T\Delta,$$

which proves (5.19).

Remark 5.1. *Using* (5.16) *and* $\varrho(\varsigma, s) = H(2H-1)(s-\varsigma)^{2H-2}$, *condition* (5.18) *is equivalent to*

$$c_1 \ge \frac{19c_3^2}{2}H(2H-1)\int_0^s \exp\left(-\frac{c_1c_2}{2}u\right)u^{2H-2}\,\mathrm{d}u, \qquad 0 \le s \le T.$$

Since the right-hand side is increasing in s, it is sufficient to verify this condition at $s = T$.

6. Conclusions

In this manuscript, we have studied the numerical approximation of the general class (3.1) of SDEs driven by fractional Brownian motion with Hurst parameter $H > \frac{1}{2}$ and a square-root term in the diffusion coefficient. Applying the Lamperti transform to convert the non-Lipschitz diffusion into additive fractional noise, we obtained SDE (3.2) with a generally stiff drift. We approximated the solution of this transformed equation by the drift-implicit Euler-Maruyama scheme. Under Assumptions 3.1–3.4, we proved that this scheme converges with mean-square order one. Moreover, we proved that when transformed back, the approximations converge under the additional moment condition of Corollary 4.1 with strong order 1 to the original square-root process.

In three examples motivated by mathematical finance, we showed how the general convergence results can be applied. The numerical experiments confirmed the predicted first-order behavior for the transformed and the original processes.

Author contributions

Minoo Kamrani: Writing–original draft, Writing–review & editing; Kristian Debrabant: Writing–review & editing. All authors have read and approved the final version of the manuscript for publication.

Use of Generative-AI tools declaration

The authors used ChatGPT (OpenAI) to assist with language editing, improving clarity and presentation. ChatGPT was also used to assist with the development and checking of LaTeX code and the MATLAB code used for the numerical experiments. All AI-assisted suggestions were reviewed and verified by the authors. The authors take full responsibility for the content of the manuscript.

Acknowledgments

The work of the first author was supported by the Iran National Science Foundation (INSF) under project No. 4046763.

Conflict of interest

The authors declare no competing interests.

References

1. V. N. Afanas'ev, V. B. Kolmanovskii, V. R. Nosov, *Mathematical theory of control systems design*, Dordrecht: Springer, 1996. https://doi.org/10.1007/978-94-017-2203-2
2. S. Busenberg, K. L. Cooke, The effect of integral conditions in certain equations modelling epidemics and population growth, *J. Math. Biol.*, **10** (1980), 13–32. https://doi.org/10.1007/BF00276393
3. M. Kamrani, Numerical solution of stochastic fractional differential equations, *Numer. Algorithms*, **68** (2015), 81–93. https://doi.org/10.1007/s11075-014-9839-7
4. A. Alfonsi, Strong order one convergence of a drift implicit Euler scheme: application to the CIR process, *Stat. Probab. Lett.*, **83** (2013), 602–607. https://doi.org/10.1016/j.spl.2012.10.034
5. A. Berkaoui, M. Bossy, A. Diop, Euler scheme for SDEs with non-Lipschitz diffusion coefficient: strong convergence, *ESAIM Probab. Stat.*, **12** (2008), 1–11. https://doi.org/10.1051/ps:2007030
6. D. J. Higham, X. R. Mao, A. M. Stuart, Strong convergence of Euler-type methods for nonlinear stochastic differential equations, *SIAM J. Numer. Anal.*, **40** (2002), 1041–1063. https://doi.org/10.1137/S0036142901389530
7. A. Alfonsi, On the discretization schemes for the CIR (and squared Bessel) processes, *Monte Carlo Methods Appl.*, **11** (2005), 355–384. https://doi.org/10.1515/156939605777438569
8. J. C. Cox, J. E. Ingersoll Jr., S. A. Ross, A theory of the term structure of interest rates, *Econometrica*, **53** (1985), 385–407. https://doi.org/10.2307/1911242

9. Y. Z. Hu, D. Nualart, X. M. Song, A singular stochastic differential equation driven by fractional Brownian motion, *Stat. Probab. Lett.*, **78** (2008), 2075–2085. https://doi.org/10.1016/j.spl.2008.01.080
10. D. Nualart, B. Saussereau, Malliavin calculus for stochastic differential equations driven by a fractional Brownian motion, *Stoch. Process. Appl.*, **119** (2009), 391–409. https://doi.org/10.1016/j.spa.2008.02.016
11. J. Gatheral, T. Jaisson, M. Rosenbaum, Volatility is rough, *Quant. Finance*, **18** (2018), 933–949. https://doi.org/10.1080/14697688.2017.1393551
12. X. H. Wang, W. L. Xiao, J. Yu, Modeling and forecasting realized volatility with the fractional Ornstein-Uhlenbeck process, *J. Econom.*, **232** (2023), 389–415. https://doi.org/10.1016/j.jeconom.2021.08.001
13. A. Chronopoulou, F. G. Viens, Estimation and pricing under long-memory stochastic volatility, *Ann. Finance*, **8** (2012), 379–403. https://doi.org/10.1007/s10436-010-0156-4
14. A. Chronopoulou, F. G. Viens, Stochastic volatility and option pricing with long-memory in discrete and continuous time, *Quant. Finance*, **12** (2012), 635–649. https://doi.org/10.1080/14697688.2012.664939
15. F. Comte, E. Renault, Long memory in continuous-time stochastic volatility models, *Math. Finance*, **8** (1998), 291–323. https://doi.org/10.1111/1467-9965.00057
16. E. Alòs, Y. Yang, A fractional Heston model with $H > 1/2$, *Stochastics*, **89** (2017), 384–399. https://doi.org/10.1080/17442508.2016.1218496
17. Y. Mishura, A. Yurchenko-Tytarenko, Fractional Cox-Ingersoll-Ross process with non-zero "mean", *Mod. Stoch. Theory Appl.*, **5** (2018), 99–111. https://doi.org/10.15559/18-VMSTA97
18. Y. Mishura, A. Yurchenko-Tytarenko, Approximating expected value of an option with non-Lipschitz payoff in fractional Heston-type model, *Int. J. Theoret. Appl. Finance*, **23** (2020), 2050031. https://doi.org/10.1142/S0219024920500314
19. Y. Mishura, G. Shevchenko, The rate of convergence for Euler approximations of solutions of stochastic differential equations driven by fractional Brownian motion, *Stochastics*, **80** (2008), 489–511. https://doi.org/10.1080/17442500802024892
20. A. Neuenkirch, Optimal approximation of SDE's with additive fractional noise, *J. Complex.*, **22** (2006), 459–474. https://doi.org/10.1016/j.jco.2006.02.001
21. A. Neuenkirch, I. Nourdin, Exact rate of convergence of some approximation schemes associated to SDEs driven by a fractional Brownian motion, *J. Theoret. Probab.*, **20** (2007), 871–899. https://doi.org/10.1007/s10959-007-0083-0
22. X. Y. Gao, J. Q. Wang, Y. X. Wang, H. F. Yang, The truncated Euler-Maruyama method for CIR model driven by fractional Brownian motion, *Stat. Probab. Lett.*, **189** (2022), 109573. https://doi.org/10.1016/j.spl.2022.109573
23. J. He, S. B. Gao, W. J. Zhan, Q. Guo, Truncated Euler-Maruyama method for stochastic differential equations driven by fractional Brownian motion with super-linear drift coefficient, *Int. J. Comput. Math.*, **100** (2023), 2184–2195. https://doi.org/10.1080/00207160.2023.2266757

24. J. L. Hong, C. Y. Huang, M. Kamrani, X. Wang, Optimal strong convergence rate of a backward Euler type scheme for the Cox-Ingersoll-Ross model driven by fractional Brownian motion, *Stoch. Process. Appl.*, **130** (2020), 2675–2692. https://doi.org/10.1016/j.spa.2019.07.014

25. M. Kamrani, E. Hausenblas, An adaptive positive preserving numerical scheme based on splitting method for the solution of the CIR model, *Math. Comput. Simul.*, **229** (2025), 673–689. https://doi.org/10.1016/j.matcom.2024.10.021

26. S. Q. Zhang, C. G. Yuan, Stochastic differential equations driven by fractional Brownian motion with locally Lipschitz drift and their implicit Euler approximation, *Proc. Roy. Soc. Edinburgh Sect. A*, **151** (2021), 1278–1304. https://doi.org/10.1017/prm.2020.60

27. G. Di Nunno, Y. Mishura, A. Yurchenko-Tytarenko, Drift-implicit Euler scheme for sandwiched processes driven by Hölder noises, *Numer. Algorithms*, **93** (2023), 459–491. https://doi.org/10.1007/s11075-022-01424-6

28. R. B. Davies, D. S. Harte, Tests for Hurst effect, *Biometrika*, **74** (1987), 95–101. https://doi.org/10.1093/biomet/74.1.95

29. P. E. Kloeden, E. Platen, *Numerical solution of stochastic differential equations*, Berlin, Heidelberg: Springer, 1992. https://doi.org/10.1007/978-3-662-12616-5

30. K. C. Chan, G. A. Karolyi, F. A. Longstaff, A. B. Sanders, An empirical comparison of alternative models of the short-term interest rate, *J. Finance*, **47** (1992), 1209–1227. https://doi.org/10.1111/j.1540-6261.1992.tb04011.x

31. S. L. Heston, *A simple new formula for options with stochastic volatility*, Course notes, Washington University, 1997.



AIMS Press

© 2026 the Author(s), licensee AIMS Press. This is an open access article distributed under the terms of the Creative Commons Attribution License (https://creativecommons.org/licenses/by/4.0)